19
Resonant Conversion

Part V of this text deals with a class of converters whose operation differs significantly from the PWM converters covered in Parts I to IV. *Resonant power converters* [1–36] contain resonant *L–C* networks whose voltage and current waveforms vary sinusoidally during one or more subintervals of each switching period. These sinusoidal variations are large in magnitude, and hence the small ripple approximation introduced in Chapter 2 does not apply.

Dc-to-high-frequency-ac inverters are required in a variety of applications, including electronic ballasts for gas discharge lamps [3,4], induction heating, and electrosurgical generators. These applications typically require generation of a sinusoid of tens or hundreds of kHz, having moderate or low total harmonic distortion. A simple resonant inverter system is illustrated in Fig. 19.1(a). A switch network produces a square wave voltage $v_s(t)$. As illustrated in Fig. 19.2, the spectrum of $v_s(t)$ contains fundamental plus odd harmonics. This voltage is applied to the input terminals of a resonant tank network. The tank network resonant frequency f_0 is tuned to the fundamental component of $v_s(t)$, that is, to the switching frequency f_s, and the tank exhibits negligible response at the harmonics of f_s. In consequence, the tank current $i_s(t)$, as well as the load voltage $v(t)$ and load current $i(t)$, have essentially sinusoidal waveforms of frequency f_s, with negligible harmonics. By changing the switching frequency f_s (closer to or further from the resonant frequency f_0), the magnitudes of $i_s(t)$, $v(t)$, and $i(t)$ can be controlled. Other schemes for control of the output voltage, such as phase-shift control of the bridge switch network, are also possible. A variety of resonant tank networks can be employed; Fig. 19.1(b) to (d) illustrate the well-known *series*, *parallel*, and *LCC* tank networks. Inverters employing the series resonant tank network are known as the *series resonant*, or *series loaded*, inverter. In the *parallel resonant* or *parallel loaded* inverter, the load voltage is equal to the resonant tank capacitor voltage. The LCC inverter employs tank capacitors both in series and in parallel with the load.

Figure 19.3 illustrates a high-frequency inverter of an electronic ballast for a gas-discharge lamp. A half-bridge configuration of the LCC inverter drives the lamp with an approximately sinusoidal

R. W. Erickson et al., *Fundamentals of Power Electronics*

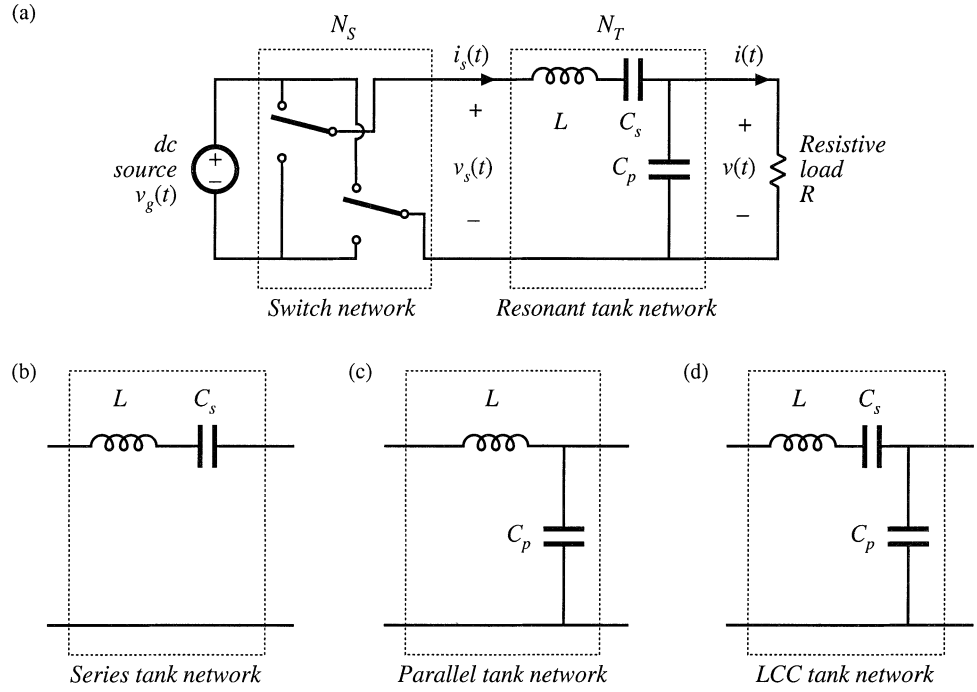

Fig. 19.1 A basic class of resonant inverters that consist of (a) a switch network N_S that drives a resonant tank network N_T near resonance. Several common tank networks: (b) series, (c) parallel, (d) LCC.

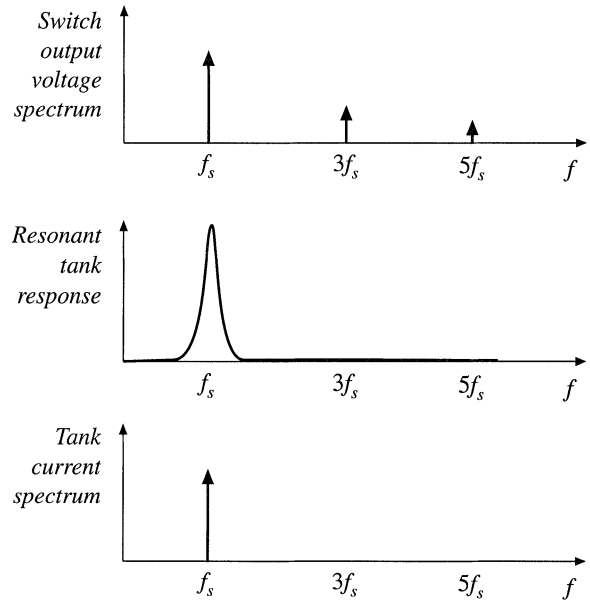

Fig. 19.2 The tank network responds primarily to the fundamental component of the applied waveforms.

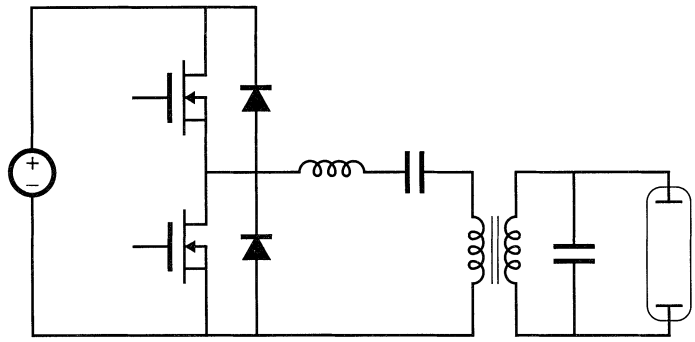

Fig. 19.3 Half-bridge LCC inverter circuit, as an electronic ballast for a gas-discharge lamp.

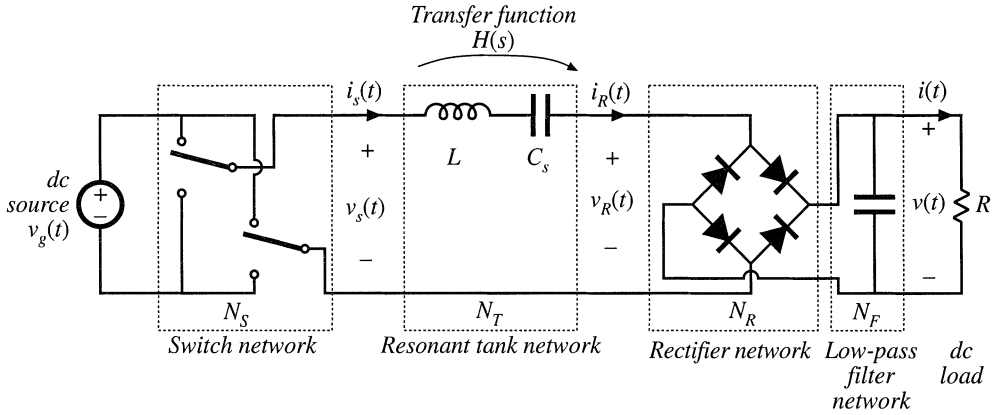

Fig. 19.4 Derivation of a resonant dc–dc converter, by rectification and filtering of the output of a resonant inverter.

high-frequency ac waveform. The converter is controlled to provide a relatively high voltage to start the lamp, and a lower voltage thereafter. When the ballast is powered by the ac utility, a low-harmonic rectifier typically provides the input dc voltage for the inverter.

A resonant dc–dc converter can be constructed by rectifying and filtering the ac output of a resonant inverter. Figure 19.4 illustrates a series-resonant dc-dc converter, in which the approximately sinusoidal resonant tank output current $i_R(t)$ is rectified by a diode bridge rectifier, and filtered by a large capacitor to supply a dc load having current I and voltage V. Again, by variation of the switching frequency f_s (closer to or further from the resonant frequency f_0), the magnitude of the tank current $i_R(t)$, and hence also the dc load current I, can be controlled. Resonant dc–dc converters based on series, parallel, LCC, and other resonant tank networks are well understood. These converters are employed when specialized application requirements justify their use. For example, they are commonly employed in high voltage dc power supplies [5,6], because the substantial leakage inductance and winding capacitance of high-voltage transformers leads unavoidably to a resonant tank network. The same principle can be employed to construct *resonant link* inverters or resonant link cycloconverters [7–9]; controllable switch networks are then employed on both sides of the resonant tank network.

Figure 19.5 illustrates another approach to resonant power conversion, in which resonant ele-

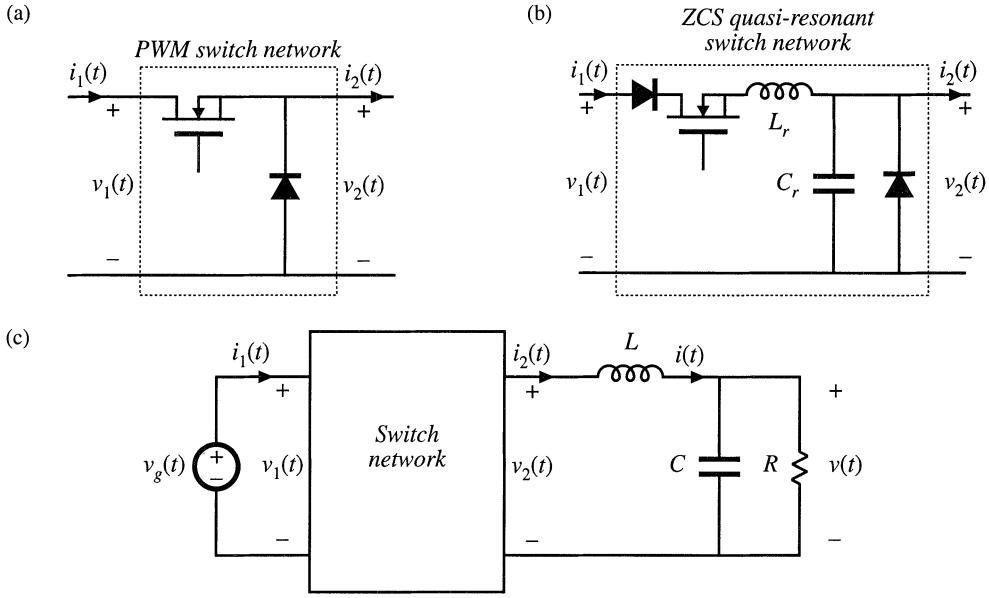

Fig. 19.5 Derivation of a quasi-resonant converter: (a) conventional PWM switch network, (b) a ZCS quasi-resonant switch network, (c) a quasi-resonant buck converter is obtained by employing a quasi-resonant switch network such as (b) in a buck converter.

ments are inserted into the switch network of an otherwise-PWM converter. A *resonant switch* network, or *quasi-resonant* converter, is then obtained. For example, in Fig. 19.5(b), resonant elements L_r and C_r are combined with the switch network transistor and diode. The resonant frequency of these elements is somewhat higher than the switching frequency. This causes the switch network waveforms $i_1(t)$ and $v_2(t)$ to become quasi-sinusoidal pulses. The resonant switch network of Fig. 19.5(b) can replace the PWM switch network of Fig. 19.5(a) in nearly any PWM converter. For example, insertion of the resonant switch network of Fig. 19.5(b) into the converter circuit of Fig. 19.5(c) leads to a quasi-resonant buck converter. Numerous resonant switch networks are known, which lead to a large number of resonant switch versions of buck, boost, buck–boost, and other converters. Quasi-resonant converters are described in Chapter 20.

The chief advantage of resonant converters is their reduced switching loss, via mechanisms known as *zero-current switching* (ZCS), and *zero-voltage switching* (ZVS). The turn-on and/or turn-off transitions of the various converter semiconductor elements can occur at zero crossings of the resonant converter quasi-sinusoidal waveforms. This eliminates some of the switching loss mechanisms described in Chapter 4. Hence, switching loss is reduced, and resonant converters can operate at switching frequencies that are higher than in comparable PWM converters. Zero-voltage switching can also eliminate some of the sources of converter-generated electromagnetic interference.

Resonant converters exhibit several disadvantages. Although the resonant element values can be chosen such that good performance with high efficiency is obtained at a single operating point, typically it is difficult to optimize the resonant elements such that good performance is obtained over a wide range of load currents and input voltages. Significant currents may circulate through the tank elements, even when the load is removed, leading to poor efficiency at light load. Also, the quasi-sinusoidal waveforms of resonant converters exhibit greater peak values than those exhibited by the rectangular waveforms of PWM converters, provided that the PWM current spikes due to diode stored charge are ignored. For

these reasons, resonant converters exhibit increased conduction losses, which can offset their reduced switching losses.

In this chapter, the properties of the series, parallel, and other resonant inverters and dc–dc converters are investigated using the *sinusoidal approximation* [3, 10–12]. Harmonics of the switching frequency are neglected, and the tank waveforms are assumed to be purely sinusoidal. This allows simple equivalent circuits to be derived for the bridge inverter, tank, rectifier, and output filter portions of the converter, whose operation can be understood and solved using standard linear ac analysis. This intuitive approach is quite accurate for operation in the continuous conduction mode with a high-Q response, but becomes less accurate when the tank is operated with a low Q-factor or for operation of dc–dc resonant converters in or near the discontinuous conduction mode.

For dc–dc resonant converters, the important result of this approach is that the dc voltage conversion ratio of a continuous conduction mode resonant converter is given approximately by the ac transfer function of the tank circuit, evaluated at the switching frequency. The tank is loaded by an effective output resistance, having a value nearly equal to the output voltage divided by the output current. It is thus quite easy to determine how the tank components and circuit connections affect the converter behavior. The influence of tank component losses, transformer nonidealities, etc., on the output voltage and converter efficiency can also be found. Several resonant network theorems are presented, which allow the load dependence of conduction loss and of the zero-voltage- or zero-current-switching properties to be explained in a simple and intuitive manner.

It is found that the series resonant converter operates with a step-down voltage conversion ratio. With a 1:1 transformer turns ratio, the dc output voltage is ideally equal to the dc input voltage when the transistor switching frequency is equal to the tank resonant frequency. The output voltage is reduced as the switching frequency is increased or decreased away from resonance. On the other hand, the parallel resonant converter is capable of both step-up and step-down of voltage levels, depending on the switching frequency and the effective tank Q-factor. The exact steady-state solutions of the ideal series and parallel resonant dc–dc converters are stated in Section 19.5.

Zero-voltage switching and zero-current switching mechanisms of the series resonant converter are described in Section 19.3. In Section 19.4, the dependence of resonant inverter properties on load is examined. A simple frequency-domain approach explains why some resonant converters, over certain ranges of operating points, exhibit large circulating tank currents and low efficiency. The boundaries of zero-voltage switching and zero-current switching are also determined.

It is also possible to modify the PWM converters of the previous chapters, so that zero-current or zero-voltage switching is obtained. A number of diverse approaches are known that lead to *soft switching* in buck, boost, forward, flyback, bridge, and other topologies. Chapter 20 summarizes some of the well-known schemes, including resonant switches, quasi-square wave switches, the full-bridge zero-voltage transition converter, and zero-voltage switching in forward and flyback converters containing active-clamp snubbers. A detailed description of soft-switching mechanisms of diodes, MOSFETs, and IGBTs is also given.

19.1 SINUSOIDAL ANALYSIS OF RESONANT CONVERTERS

Consider the class of resonant converters that contain a controlled switch network N_S that drives a linear resonant tank network N_T. In a resonant inverter, the tank network drives a resistive load as in Fig. 19.1. The reactive component of the load impedance, if any, can be effectively incorporated into the tank network. In the case of a resonant dc–dc converter, the resonant tank network is connected to an uncontrolled rectifier network N_R, filter network N_F and load R, as illustrated in Fig. 19.4. Many well-known converters can be represented in this form, including the series, parallel, and LCC topologies.

In the most common modes of operation, the controlled switch network produces a square wave voltage output $v_s(t)$ whose frequency f_s is close to the tank network resonant frequency f_0. In response, the tank network rings with approximately sinusoidal waveforms of frequency f_s. In the case where the resonant tank responds primarily to the fundamental component f_s of the switch waveform $v_s(t)$, and has negligible response at the harmonic frequencies nf_s, n = 3, 5, 7,..., then the tank waveforms are well approximated by their fundamental components. As shown in Fig. 19.2, this is indeed the case when the tank network contains a high-Q resonance at or near the switching frequency, and a low-pass characteristic at higher frequencies. Hence, let us neglect harmonics, and compute the relationships between the fundamental components of the tank terminal waveforms $v_s(t)$, $i_s(t)$, $i_R(t)$, and $v_R(t)$.

19.1.1 Controlled Switch Network Model

If the switch network of Fig. 19.6 is controlled to produce a square wave of frequency $f_s = \omega_s/2\pi$ as in Fig. 19.7, then its output voltage waveform $v_s(t)$ can be expressed in the Fourier series

$$v_s(t) = \frac{4V_g}{\pi} \sum_{n=1,3,5,\ldots} \frac{1}{n} \sin(n\omega_s t) \tag{19.1}$$

The fundamental component is

$$v_{s1}(t) = \frac{4V_g}{\pi} \sin(\omega_s t) = V_{s1} \sin(\omega_s t) \tag{19.2}$$

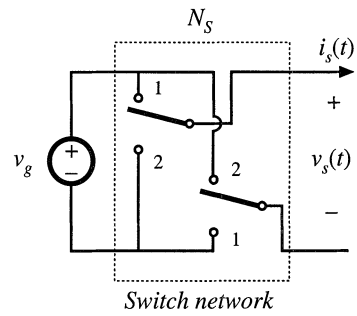

Fig. 19.6 An ideal switch network.

which has a peak amplitude of $(4/\pi)$ times the dc input voltage V_g, and is in phase with the original square wave $v_s(t)$. Hence, the switch network output terminal is modeled as a sinusoidal voltage generator, $v_{s1}(t)$.

It is also of interest to model the converter dc input port. This requires computation of the dc component I_g of the switch input current $i_g(t)$. The switch input current $i_g(t)$ is equal to the output current $i_s(t)$ when the switches are in position 1, and its inverse $-i_s(t)$ when the switches are in position 2. Under the conditions described above, the tank rings sinusoidally and $i_s(t)$ is well approximated by a sinusoid of some peak amplitude I_{s1} and phase φ_s:

$$i_s(t) \approx I_{s1} \sin(\omega_s t - \varphi_s) \tag{19.3}$$

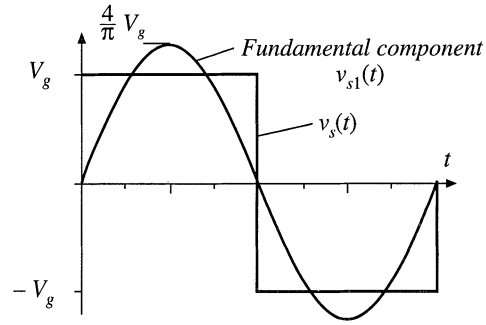

Fig. 19.7 Switch network output voltage $v_s(t)$ and its fundamental component $v_{s1}(t)$.

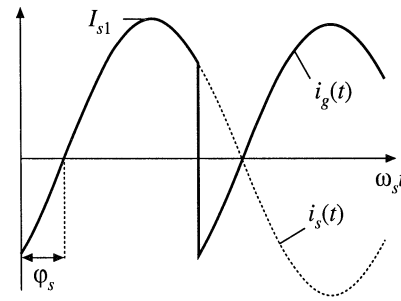

Fig. 19.8 Switch network waveforms $i_s(t)$ and $i_g(t)$.

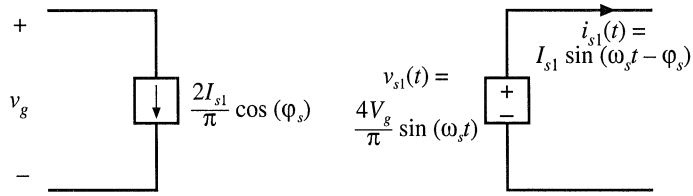

Fig. 19.9 An equivalent circuit for the switch network, which models the fundamental component of the output voltage waveform and the dc component of the input current waveform.

The input current waveform is shown in Fig. 19.8.

The dc component, or average value, of the input current can be found by averaging $i_g(t)$ over one half switching period:

$$\begin{aligned}\left\langle i_g(t)\right\rangle_{T_s} &= \frac{2}{T_s}\int_0^{T_s/2} i_g(\tau)d\tau \\ &\approx \frac{2}{T_s}\int_0^{T_s/2} I_{s1}\sin(\omega_s\tau - \varphi_s)d\tau \\ &= \frac{2}{\pi} I_{s1}\cos(\varphi_s)\end{aligned} \tag{19.4}$$

Thus, the dc component of the converter input current depends directly on the peak amplitude of the tank input current I_{s1} and on the cosine of its phase shift φ_s.

An equivalent circuit for the switch is given in Fig. 19.9. This circuit models the basic energy conversion properties of the switch: the dc power supplied by the voltage source V_g is converted into ac power at the switch output. Note that the dc power at the source is the product of V_g and the dc component of $i_g(t)$, and the ac power at the switch is the average of $v_s(t)i_s(t)$. Furthermore, if the harmonics of $v_s(t)$ are negligible, then the switch output voltage can be represented by its fundamental component, a sinusoid $v_{s1}(t)$ of peak amplitude $4V_g/\pi$. It can be verified that the switch network dc input power and fundamental average output power, predicted by Fig. 19.9, are equal.

19.1.2 Modeling the Rectifier and Capacitive Filter Networks

In the series resonant dc–dc converter, the output rectifier is driven by the nearly sinusoidal tank output current $i_R(t)$. A large capacitor C_F is placed at the dc output, so that the output voltage $v(t)$ contains negligible harmonics of the switching frequency f_s, as shown in Fig. 19.10. Hence, we can make the small-rip-

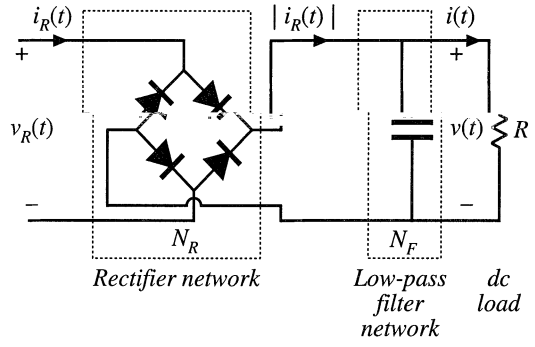

Fig. 19.10 Uncontrolled rectifier with capacitive filter network, as in the series resonant converter.

ple approximation as usual: $v(t) \approx V$, $i(t) \approx I$. The diode rectifiers switch when $i_R(t)$ passes through zero, as shown in Fig. 19.11. The rectifier input voltage $v_R(t)$ is essentially a square wave, equal to + $v(t)$ when $i_R(t)$ is positive and – $v(t)$ when $i_R(t)$ is negative. Note that $v_R(t)$ is in phase with $i_R(t)$.

If the tank output current $i_R(t)$ is a sinusoid with peak amplitude I_{R1} and phase shift φ_R:

$$i_R(t) = I_{R1} \sin(\omega_s t - \varphi_R) \tag{19.5}$$

then the rectifier input voltage may be expressed in the Fourier series

$$v_R(t) = \frac{4V}{\pi} \sum_{n=1,3,5,\ldots}^{\infty} \frac{1}{n} \sin(n\omega_s t - \varphi_R) \tag{19.6}$$

where φ_R is the phase shift of $i_R(t)$, with respect to $v_s(t)$. This voltage waveform is impressed on the output port of the resonant tank network. Again, if the tank network responds primarily to the fundamental component (f_s) of $v_R(t)$, and has negligible response at the harmonic frequencies nf_s, n = 3, 5, 7..., then the harmonics of $v_R(t)$ can be ignored. The voltage waveform $v_R(t)$ is then well approximated by its fundamental component $v_{R1}(t)$:

$$v_{R1}(t) = \frac{4V}{\pi} \sin(\omega_s t - \varphi_R) = V_{R1} \sin(\omega_s t - \varphi_R) \tag{19.7}$$

The fundamental voltage component $v_{R1}(t)$ has a peak value of $(4/\pi)$ times the dc output voltage V, and is in phase with the current $i_R(t)$.

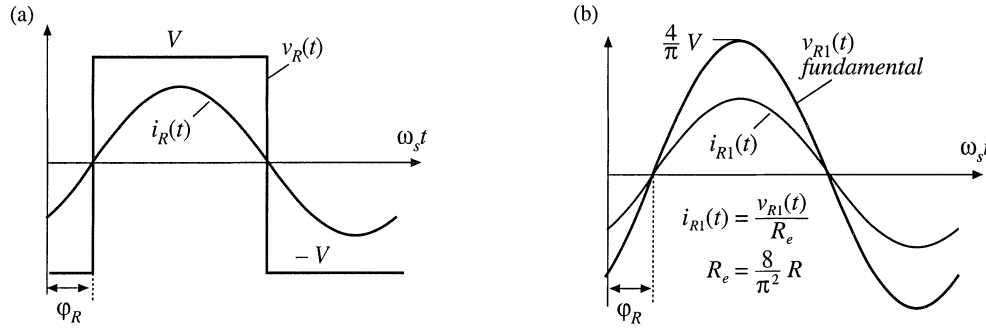

Fig. 19.11 Rectifier network input terminal waveforms: (a) actual waveforms $v_R(t)$ and $i_R(t)$, (b) fundamental components $v_{R1}(t)$ and $i_{R1}(t)$.

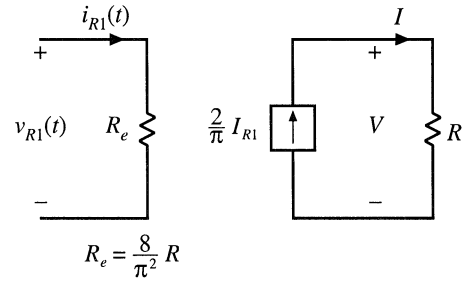

Fig. 19.12 An equivalent circuit for the rectifier and filter network, which models the fundamental components of the rectifier ac input waveforms and the dc components of the load waveforms. The rectifier presents an effective resistive load R_e to the tank network.

The rectified tank output current, $|\, i_R(t)\,|$, is filtered by capacitor C_F. Since no dc current can pass through C_F, the dc component of $|\, i_R(t)\,|$ must be equal to the steady-state load current I. By equating dc components we obtain:

$$\begin{aligned} I &= \frac{2}{T_S} \int_0^{T_s/2} I_{R1} \left| \sin(\omega_s t - \varphi_R) \right| dt \\ &= \frac{2}{\pi} I_{R1} \end{aligned} \tag{19.8}$$

Therefore, the load current and the tank output current amplitudes are directly related in steady state.

Since $v_{R1}(t)$, the fundamental component of $v_R(t)$, is in phase with $i_R(t)$, the rectifier presents an effective resistive load R_e to the tank circuit. The value of R_e is equal to the ratio of $v_{R1}(t)$ to $i_R(t)$. Division of Eq. (19.7) by Eq. (19.5), and elimination of I_{R1} using Eq. (19.8) yields

$$R_e = \frac{v_{R1}(t)}{i_R(t)} = \frac{8}{\pi^2} \frac{V}{I} \tag{19.9}$$

With a resistive load R equal to V/I, this equation reduces to

$$R_e = \frac{8}{\pi^2} R = 0.8106R \tag{19.10}$$

Thus, the tank network is damped by an effective load resistance R_e equal to 81% of the actual load resistance R. An equivalent circuit that models the rectifier network input port fundamental components and output port dc components is given in Fig. 19.12.

19.1.3 Resonant Tank Network

We have postulated that the effects of harmonics can be neglected, and we have consequently shown that the bridge can be modeled as a fundamental voltage source $v_{s1}(t)$. In the case of a dc-dc converter, the rectifier can be modeled using an effective resistor of value R_e. We can now solve the resonant tank network by standard linear analysis.

As shown in Fig. 19.13, the tank circuit is a linear network with the following voltage transfer function:

$$\frac{v_{R1}(s)}{v_{s1}(s)} = H(s) \tag{19.11}$$

Hence, the ratio V_{R1}/V_{s1} of the peak magnitudes of $v_{R1}(t)$ and $v_{s1}(t)$ is given by:

$$\frac{V_{R1}}{V_{s1}} = \left\| H(s) \right\|_{s = j\omega_s} \tag{19.12}$$

In addition, $i_R(s)$ is given by:

$$i_R(s) = \frac{v_{R1}(s)}{R_e} = \frac{H(s)}{R_e} v_{s1}(s) \tag{19.13}$$

So the peak magnitude of $i_R(t)$ is:

$$I_{R1} = \frac{\left\| H(s) \right\|_{s = j\omega_s}}{R_e} V_{s1} \tag{19.14}$$

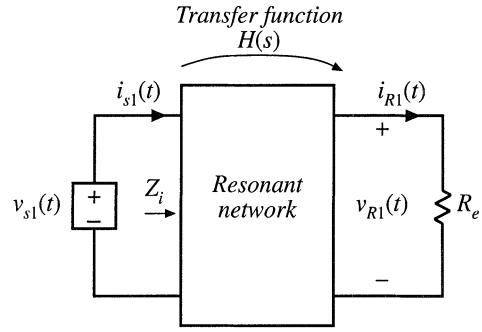

Fig. 19.13 The linear tank network, excited by an effective sinusoidal input source and driving an effective resistive load.

Thus, the magnitude of the tank transfer function is found, with an effective resistive load.

19.1.4 Solution of Converter Voltage Conversion Ratio $M = V/V_g$

An equivalent circuit of a complete dc–dc resonant converter is depicted in Fig. 19.14. The voltage conversion ratio of the resonant converter can now be found:

$$M = \frac{V}{V_g} = \underbrace{(R)}_{\left(\frac{V}{I}\right)} \underbrace{\left(\frac{2}{\pi}\right)}_{\left(\frac{I}{I_{R1}}\right)} \underbrace{\left(\frac{1}{R_e}\right)}_{\left(\frac{I_{R1}}{V_{R1}}\right)} \underbrace{\left(\left\| H(s) \right\|_{s = j\omega_s}\right)}_{\left(\frac{V_{R1}}{V_{s1}}\right)} \underbrace{\left(\frac{4}{\pi}\right)}_{\left(\frac{V_{s1}}{V_g}\right)} \tag{19.15}$$

Simplification by use of Eq. (19.10) yields:

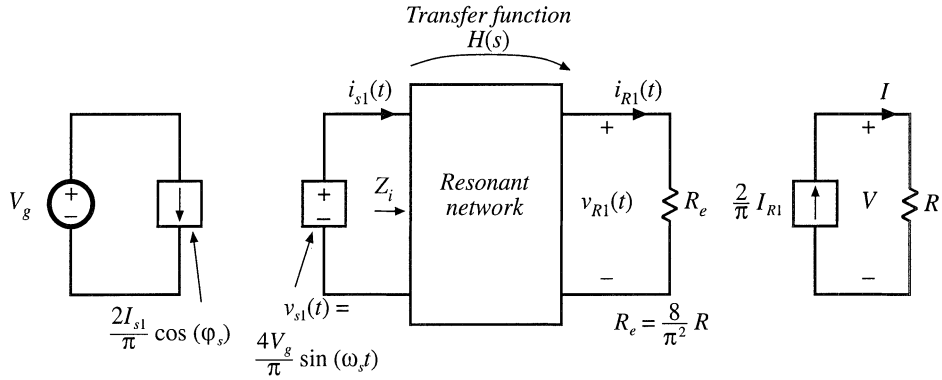

Fig. 19.14 Steady-state equivalent circuit that models the dc and fundamental components of resonant converter waveforms.

$$\frac{V}{V_g} = \left\| H(s) \right\|_{s = j\omega_s} \tag{19.16}$$

Equation (19.16) is the desired result. It states that the dc conversion ratio of the resonant converter is approximately the same as the ac transfer function of the resonant tank circuit, evaluated at the switching frequency f_s. This intuitive result can be applied to converters with many different types of tank circuits. However, it should be reemphasized that Eq. (19.16) is valid only if the response of the tank circuit to the harmonics of $v_s(t)$ is negligible compared to the fundamental response, an assumption that is not always justified. In addition, we have assumed that the switch network is controlled to produce a square wave and that the rectifier network drives a capacitive-type filter network. Finally, the transfer function $H(s)$ is evaluated using the effective load resistance R_e given by Eq. (19.9).

19.2 EXAMPLES

19.2.1 Series Resonant DC–DC Converter Example

The series resonant converter with switching frequency control is shown in Fig. 19.4. Current-bidirectional two-quadrant switches are necessary. For this circuit, the tank network consists of a series L–C circuit, and Fig. 19.14 can be redrawn as in Fig. 19.15. The transfer function $H(s)$ is therefore:

$$\begin{aligned} H(s) &= \frac{R_e}{Z_i(s)} = \frac{R_e}{R_e + sL + \frac{1}{sC}} \\ &= \frac{\left(\frac{s}{Q_e\omega_0}\right)}{1 + \left(\frac{s}{Q_e\omega_0}\right) + \left(\frac{s}{\omega_0}\right)^2} \end{aligned} \tag{19.17}$$

where

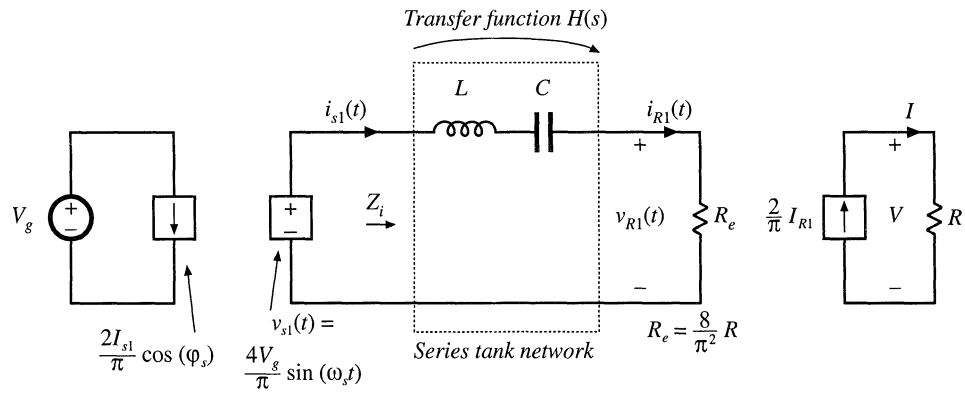

Fig. 19.15 Steady-state equivalent circuit of the series resonant converter.

$$\omega_0 = \frac{1}{\sqrt{LC}} = 2\pi f_0$$
$$R_0 = \sqrt{\frac{L}{C}}$$
$$Q_e = \frac{R_0}{R_e}$$

The magnitude of $H(j\omega_s)$, which coincides with the converter dc conversion ratio $M = V/V_g$, is

$$M = \left\| H(j\omega_s) \right\| = \frac{1}{\sqrt{1 + Q_e^2 \left(\frac{1}{F} - F \right)^2}} \tag{19.18}$$

where

$$F = f_s / f_0 \tag{19.19}$$

The Bode diagrams of $Z_i(s)$ and $H(s)$ are constructed in Fig. 19.16, using the graphical construction method of Chapter 8. The series resonant impedance $Z_i(s)$ is dominated by the capacitor C at low frequency, and by the inductor L at high frequency. At the resonant frequency f_0, the impedances of the inductor and capacitor are equal in magnitude and opposite in phase; hence, they cancel. The series resonant impedance $Z_i(s)$ is equal to R_e at $f = f_0$.

The transfer function $\| H(j\omega) \|$ is constructed graphically, by division of R_e by the $\| Z_i \|$ asymptotes of Fig. 19.16. At resonance, one obtains $\| H \| = R_e/R_e = 1$. At frequencies above or below the resonant frequency, $\| Z_i \| > R_e$ and hence $\| H \| < 1$. So the conversion ratio M is less than or equal to 1. It can also be seen that a decrease in the load resistance R, which increases the effective quality factor Q_e, causes a more peaked response in the vicinity of resonance. Exact characteristics of the series resonant converter are plotted in Fig. 19.45.

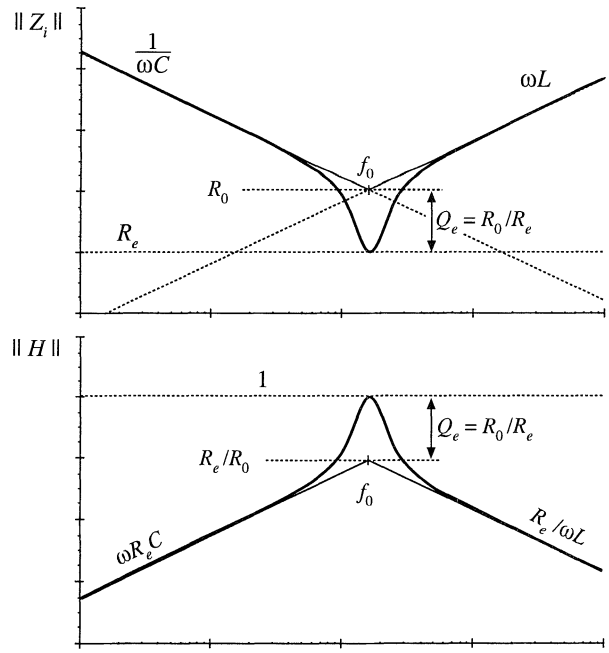

Fig. 19.16 Construction of the Bode diagrams of $Z_i(s)$ and $H(s)$ for the series resonant converter.

Over what range of switching frequencies is Eq. (19.18) accurate? The response of the tank to the fundamental component of $v_s(t)$ must be sufficiently greater than the response to the harmonics of $v_s(t)$. This is certainly true for operation above resonance because $H(s)$ contains a bandpass characteristic that decreases with a single pole slope for $f_s > f_0$. For the same reason, Eq. (19.18) is valid when the switching frequency is below but near resonance.

However, for switching frequencies f_s much less than the resonant frequency f_0, the sinusoidal approximation breaks down completely because the tank responds more strongly to the harmonics of

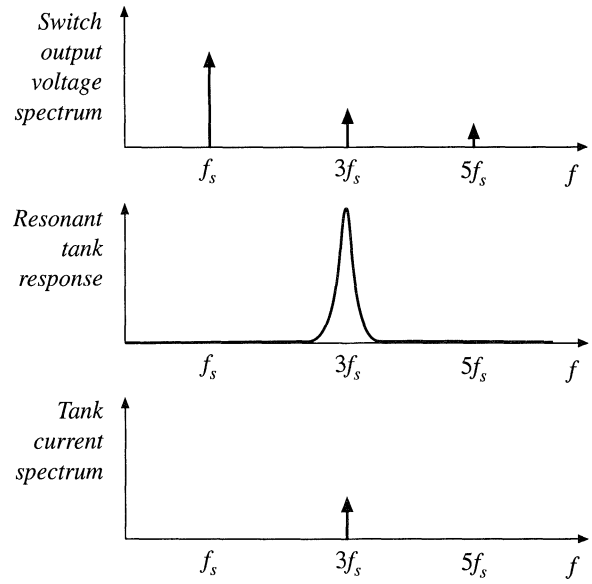

Fig. 19.17 Excitation of the tank network by the third harmonic of the switching frequency.

$v_s(t)$ than to its fundamental. For example, at $f_s = f_0/3$, the third harmonic of $v_s(t)$ is equal to f_0 and directly excites the tank resonance. Some other type of analysis must be used to understand what happens at these lower frequencies. Also, in the low-Q case, the approximation is less accurate because the filter response is less peaked, and hence does not favor the fundamental component as strongly. As shown in a later section, discontinuous conduction modes may then occur whose waveforms are highly nonsinusoidal.

19.2.2 Subharmonic Modes of the Series Resonant Converter

If the n^{th} harmonic of the switch output waveform $v_s(t)$ is close to the resonant tank frequency, $nf_s \sim f_0$, and if the tank effective quality factor Q_e is sufficiently large, then as illustrated in Fig. 19.17, the tank responds primarily to harmonic n. All other components of the tank waveforms can then be neglected, and it is a good approximation to replace $v_s(t)$ with its n^{th} harmonic component:

$$v_s(t) \approx v_{sn}(t) = \frac{4V_g}{n\pi} \sin(n\omega_s t) \tag{19.20}$$

This expression differs from Eq. (19.2) because the amplitude is reduced by a factor of $1/n$, and the fre-

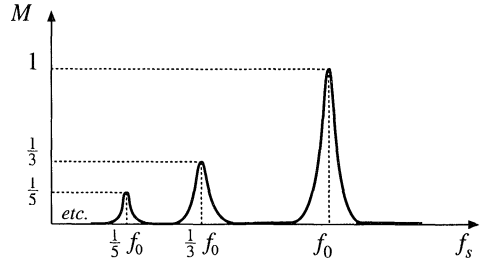

Fig. 19.18 The subharmonic modes of the series resonant converter. These modes occur when the harmonics of the switching frequency excite the tank resonance.

quency is nf_s rather than f_s.

The arguments used to model the tank and rectifier/filter networks are unchanged from Section 19.1. The rectifier presents an effective resistive load to the tank, of value $R_e = 8R/\pi^2$. In consequence, the converter dc conversion ratio is given by

$$M = \frac{V}{V_g} = \frac{\left\| H(jn\omega_s) \right\|}{n} \tag{19.21}$$

This is a good approximation provided that nf_s is close to f_0, and that Q_e is sufficiently large. Typical characteristics are sketched in Fig. 19.18.

The series resonant converter is not generally designed to operate in a subharmonic mode, since the fundamental modes yield greater output voltage and power, and hence higher efficiency. Nonetheless, the system designer should be aware of their existence, because inadvertent operation in these modes can lead to large signal instabilities.

19.2.3 Parallel Resonant DC–DC Converter Example

The parallel resonant dc–dc converter is diagrammed in Fig. 19.19. It differs from the series resonant converter in two ways. First, the tank capacitor appears in parallel with the rectifier network rather than in series: this causes the tank transfer function $H(s)$ to have a different form. Second, the rectifier drives an inductive-input low-pass filter. In consequence, the value of the effective resistance R_e differs from that of the rectifier with a capacitive filter. Nonetheless, sinusoidal approximations can be used to understand the operation of the parallel resonant converter.

As in the series resonant converter, the switch network is controlled to produce a square wave $v_s(t)$. If the tank network responds primarily to the fundamental component of $v_s(t)$, then arguments identical to those of Section 19.1 can be used to model the output fundamental components and input dc components of the switch waveforms. The resulting equivalent circuit is identical to Fig. 19.9.

The uncontrolled rectifier with inductive filter network can be described using the dual of the arguments of Section 19.1.2. In the parallel resonant converter, the output rectifiers are driven by the nearly sinusoidal tank capacitor voltage $v_R(t)$, and the diode rectifiers switch when $v_R(t)$ passes through zero as in Fig. 19.20. If the filter inductor current ripple is small, then in steady-state the filter inductor current is essentially equal to the dc load current I. The rectifier input current $i_R(t)$ is therefore a square wave of amplitude I, and is in phase with the tank capacitor voltage $v_R(t)$:

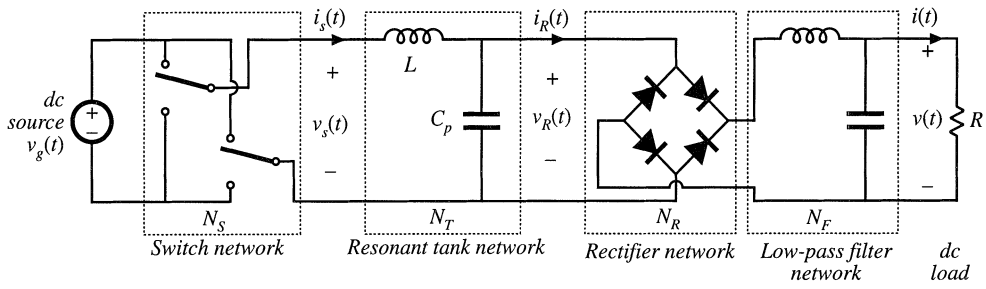

Fig. 19.19 Block diagram of the parallel resonant converter.

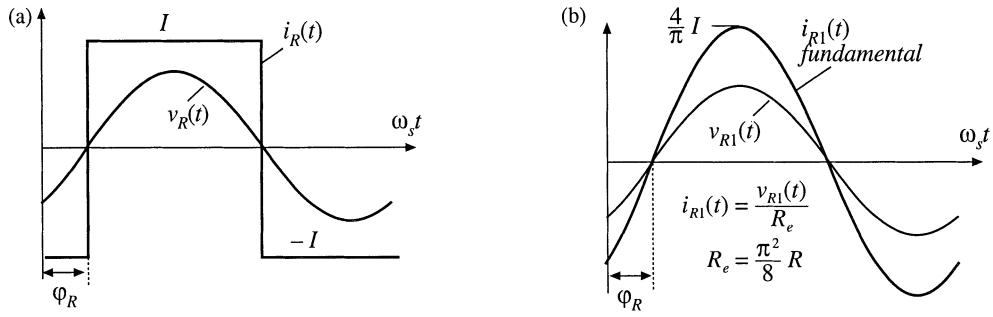

Fig. 19.20 Rectifier network input terminal waveforms, for the parallel resonant converter: (a) actual waveforms $v_R(t)$ and $i_R(t)$, (b) fundamental components $v_{R1}(t)$ and $i_{R1}(t)$.

$$i_R(t) = \frac{4I}{\pi} \sum_{n=1,3,5,\cdots}^{\infty} \frac{1}{n} \sin(n\omega_s t - \varphi_R) \tag{19.22}$$

where φ_R is the phase shift of $v_R(t)$.

The fundamental component of $i_R(t)$ is

$$i_{R1}(t) = \frac{4I}{\pi} \sin(\omega_s t - \varphi_R) \tag{19.23}$$

Hence, the rectifier again presents an effective resistive load to the tank circuit, equal to

$$R_e = \frac{v_{R1}(t)}{i_{R1}(t)} = \frac{\pi V_{R1}}{4I} \tag{19.24}$$

The ac components of the rectified tank capacitor voltage $|v_R(t)|$ are removed by the output low pass filter. In steady state, the output voltage V is equal to the dc component of $|v_R(t)|$:

$$V = \frac{2}{T_s} \int_0^{T_s/2} V_{R1} \left| \sin(\omega_s t - \varphi_R) \right| dt = \frac{2}{\pi} V_{R1} \tag{19.25}$$

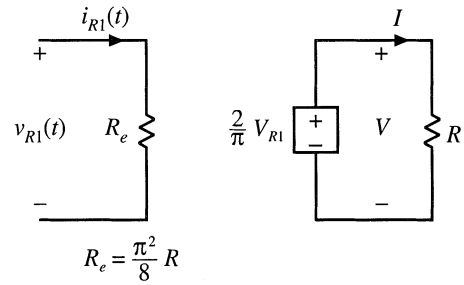

Fig. 19.21 An equivalent circuit for the rectifier and inductive filter network of the parallel resonant converter, which models the fundamental components of the rectifier ac input waveforms and the dc components of the load waveforms.

So the load voltage V and the tank capacitor voltage amplitude are directly related in steady state. Substitution of Eq. (19.25) and resistive load characteristics $V = IR$ into Eq. (19.24) yields:

$$R_e = \frac{\pi^2}{8} R = 1.2337R \tag{19.26}$$

An equivalent circuit for the uncontrolled rectifier with inductive filter network is given in Fig. 19.21. This model is similar to the one used for the series resonant converter, Fig. 19.12, except that the roles of the rectifier input voltage $v_R(t)$ and current $i_R(t)$ are interchanged, and the effective resistance R_e has a different value. The model for the complete converter is given in Fig. 19.22.

Solution of Fig. 19.22 yields the converter dc conversion ratio:

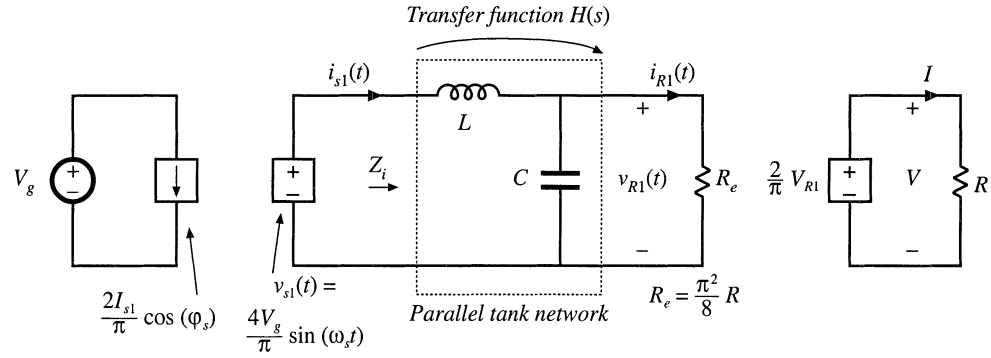

Fig. 19.22 Equivalent circuit for the parallel resonant converter, which models the fundamental components of the tank waveforms, and the dc components of the converter input current and output voltage.

$$M = \frac{V}{V_g} = \frac{8}{\pi^2} \left\| H(s) \right\|_{s = j\omega_s} \tag{19.27}$$

where $H(s)$ is the tank transfer function

$$H(s) = \frac{Z_o(s)}{sL} \tag{19.28}$$

and

$$Z_o(s) = sL \,\|\, \frac{1}{sC} \,\|\, R_e \tag{19.29}$$

The Bode magnitude diagrams of $H(s)$ and $Z_o(s)$ are constructed in Fig. 19.23, using the graphical construction method of Chapter 8. The impedance $Z_o(s)$ is the parallel combination of the impedances of the tank inductor L, capacitor C, and effective load R_e. The magnitude asymptote of the parallel combination of these components, at a given frequency, is equal to the smallest of the individual asymptotes ωL, $1/\omega C$, and R_e. Hence, at low frequency where the inductor impedance dominates the parallel combination, $\| Z_o(s) \| \cong \omega L$, while at high frequency the capacitor dominates and $\| Z_o(s) \| \cong 1/\omega C$. At resonance, the impedances of the inductor and capacitor are equal in magnitude but opposite in phase, so that their effects cancel. The impedance $\| Z_o(s) \|$ is then equal to R_e:

$$\left\| Z_o(s) \right\|_{s = j\omega_s} = \frac{1}{\frac{1}{j\omega_0 L} + j\omega_0 C + \frac{1}{R_e}} = R_e \tag{19.30}$$

with

$$\omega_0 L = \frac{1}{\omega_0 C} = R_0$$

The dc conversion ratio is therefore

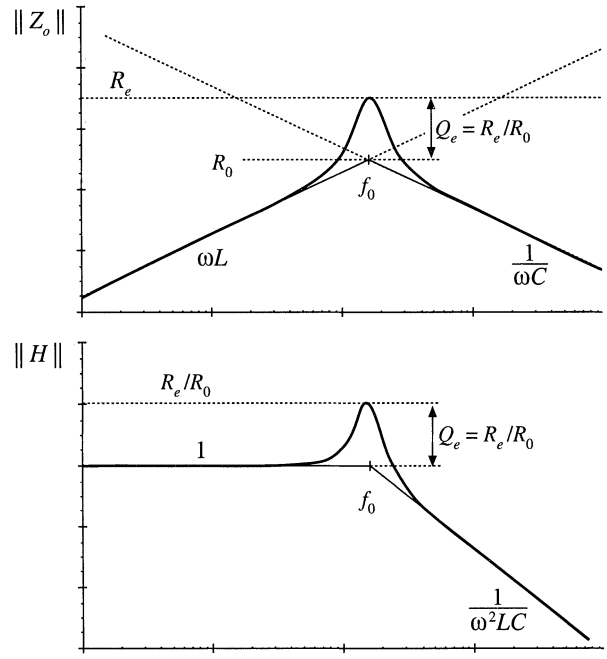

Fig. 19.23 Construction of Bode diagrams of $Z_t(s)$ and $H(s)$ for the parallel resonant converter.

$$M = \frac{8}{\pi^2}\left\| \frac{Z_o(s)}{sL} \right\|_{s=j\omega_s} = \frac{8}{\pi^2}\left\| \frac{1}{1 + \frac{s}{Q_e\omega_0} + \left(\frac{s}{\omega_0}\right)^2} \right\|_{s=j\omega_s}$$
$$= \frac{8}{\pi^2} \frac{1}{\sqrt{\left(1-F^2\right)^2 + \left(\frac{F}{Q_e}\right)^2}} \tag{19.31}$$

where $F = f_s/f_0$.

At resonance, the conversion ratio is

$$M = \frac{8}{\pi^2}\frac{R_e}{R_0} = \frac{R}{R_0} \tag{19.32}$$

The actual peak value of M occurs at a switching frequency slightly below the resonant frequency, with peak M slightly greater than Eq. (19.32). Provided that the load resistance R is greater than the tank characteristic impedance R_e, the parallel resonant converter can produce conversion ratios both greater than and less than one. In fact, the ideal parallel resonant converter can produce conversion ratios approaching infinity, provided that the output current is limited to values less than V_g/R_0. Of course, losses limit the maximum output voltage that can be produced by practical converters.

19.3 SOFT SWITCHING

As mentioned previously, the soft-switching phenomena known as zero-current switching (ZCS) and zero-voltage switching (ZVS) can lead to reduced switching loss. When the turn-on and/or turn-off tran-

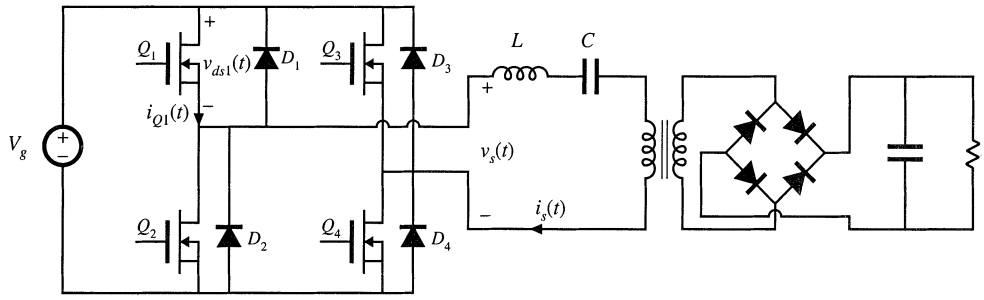

Fig. 19.24 A series resonant converter incorporating a full-bridge switch network.

sitions of a semiconductor switching device coincide with the zero crossings of the applied waveforms, some of the switching loss mechanisms discussed in Section 4.3 are eliminated. In converters containing MOSFETs and diodes, zero-voltage switching mitigates the switching loss otherwise caused by diode recovered charge and semiconductor output capacitance. Zero-current switching can mitigate the switching loss caused by current tailing in IGBTs and by stray inductances. Zero-current switching can also be used for commutation of SCRs. In the majority of applications, where diode recovered charge and semiconductor output capacitances are the dominant sources of PWM switching loss, zero-voltage switching is preferred.

19.3.1 Operation of the Full Bridge Below Resonance: Zero-Current Switching

When the series and parallel resonant inverters and dc–dc converters are operated below resonance, the zero-current switching phenomenon can occur, in which the circuit causes the transistor current to go to zero before the transistor is turned off. Let us consider the operation of the full bridge switch network of the series resonant converter in detail.

A full bridge circuit, realized using power MOSFETs and antiparallel diodes, is shown in Fig. 19.24. The switch output voltage $v_s(t)$, and its fundamental component $v_{s1}(t)$, as well as the approximately sinusoidal tank current waveform $i_s(t)$, are illustrated in Fig. 19.25. At frequencies less than the tank resonant frequency, the input impedance of the series resonant tank network $Z_i(s)$ is dominated by the tank capacitor impedance [see Fig. 19.16(a)]. Hence, the tank presents an effective capacitive load to the bridge, and switch current $i_s(t)$ leads the switch voltage fundamental component $v_{s1}(t)$, as shown in Fig. 19.25. In consequence, the zero crossing of the current waveform $i_s(t)$ occurs before the zero crossing of the voltage $v_s(t)$.

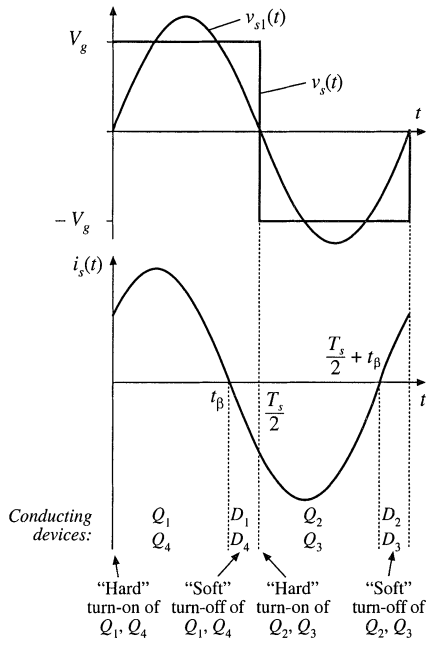

Fig. 19.25 Switch network output waveforms for the series resonant converter, operated below resonance in the $k = 1$ CCM. Zero-current switching aids the transistor turn-off process.

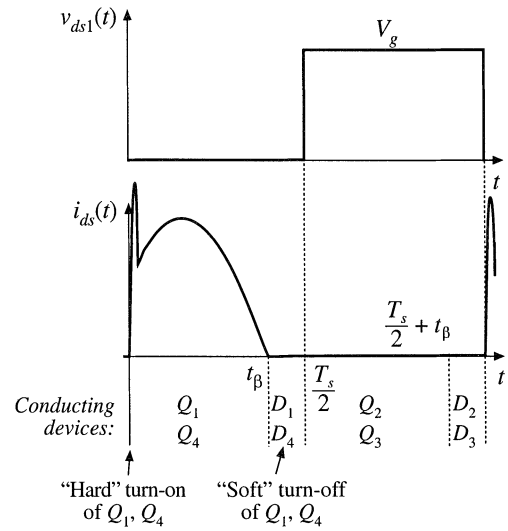

Fig. 19.26 Transistor Q_1 voltage and current waveforms, for operation of the series resonant converter below resonance in the $k = 1$ CCM.

For the half cycle $0 < t < T_s/2$, the switch voltage v_s is equal to $+ V_g$. For $0 < t < t_\beta$, the current $i_s(t)$ is positive and transistors Q_1 and Q_4 conduct. Diodes D_1 and D_4 conduct when $i_s(t)$ is negative, over the interval $t_\beta < t < T_s/2$. The situation during $T_s/2 < t < T_s$ is symmetrical. Since $i_{s1}(t)$ leads $v_{s1}(t)$, the transistors conduct before their respective antiparallel diodes. Note that, at any given time during the D_1 conduction interval $t_\beta < t < T_s/2$, transistor Q_1 can be turned off without incurring switching loss. The circuit naturally causes the transistor turn-off transition to be lossless, and long turn-off switching times can be tolerated.

In general, zero current switching can occur when the resonant tank presents an effective capacitive load to the switches, so that the switch current zero crossings occur before the switch voltage zero crossings. In the bridge configuration, zero current switching is characterized by the half-bridge conduction sequence Q_1–D_1–Q_2–D_2, such that the transistors are turned off while their respective antiparallel diodes conduct. It is possible, if desired, to replace the transistors with naturally commutated thyristors whenever the zero-current-switching property occurs at the turn-off transition.

The transistor turn-on transition in Fig. 19.26 is similar to that of a PWM switch: it is hard-switched and is not lossless. During the turn-on transition of Q_1, diode D_2 must turn off. Neither the transistor current nor the transistor voltage is zero, Q_1 passes through a period of high instantaneous power dissipation, and switching loss occurs. As in the PWM case, the reverse recovery current of diode D_2 flows through Q_1. This current spike can be the largest component of switching loss. In addition, the energy stored in the drain-to-source capacitances of Q_1 and Q_2 and in the depletion layer capacitance of D_1 is lost when Q_1 turns on. These turn-on transition switching loss mechanisms can be a major disadvantage of zero-current-switching schemes. Since zero-current switching does not address the switching loss mechanisms that dominate in MOSFET converters, improvements in efficiency are typically not observed.

19.3.2 Operation of the Full Bridge Above Resonance: Zero-Voltage Switching

When the series resonant converter is operated above resonance, the zero-voltage switching phenomenon can occur, in which the circuit causes the transistor voltage to become zero before the controller turns the

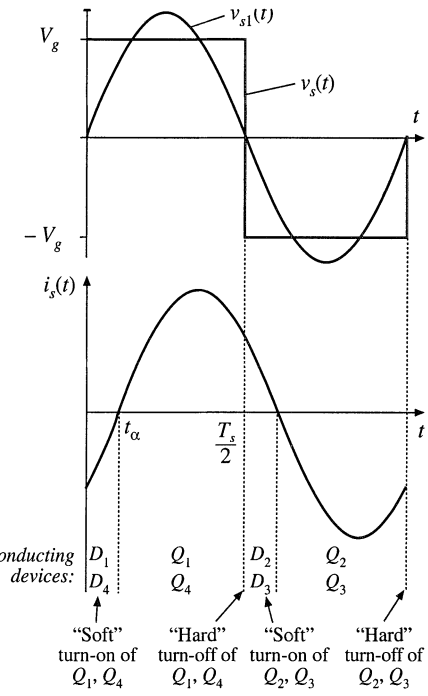

Fig. 19.27 Switch network output waveforms for the series resonant converter, operated above resonance in the continuous conduction mode. Zero-voltage switching aids the transistor turn-on process.

transistor on. With a minor circuit modification, the transistor turn-off transitions can also be caused to occur at zero voltage. This process can lead to significant reductions in the switching losses of converters based on MOSFETs and diodes.

For the full bridge circuit of Fig. 19.24, the switch output voltage $v_s(t)$, and its fundamental component $v_{s1}(t)$, as well as the approximately sinusoidal tank current waveform $i_s(t)$, are plotted in Fig. 19.27. At frequencies greater than the tank resonant frequency, the input impedance of the tank network $Z_i(s)$ is dominated by the tank inductor impedance. Hence, the tank presents an effective inductive load to the bridge, and the switch current $i_s(t)$ lags the switch voltage fundamental component $v_{s1}(t)$, as shown in Fig. 19.27. In consequence, the zero crossing of the voltage waveform $v_s(t)$ occurs before the current waveform $i_s(t)$.

For the half cycle $0 < t < T_s/2$, the switch voltage $v_s(t)$ is equal to $+V_g$. For $0 < t < t_\alpha$, the current $i_s(t)$ is negative and diodes D_1 and D_4 conduct. Transistors Q_1 and Q_4 conduct when $i_s(t)$ is positive, over the interval $t_\alpha < t < T_s/2$. The waveforms during $T_s/2 < t < T_s$ are symmetrical. Since the zero crossing of $v_s(t)$ leads the zero crossing of $i_s(t)$, the transistors conduct after their respective antiparallel diodes. Note that, at any given time during the D_1 conduction interval $0 < t < t_\alpha$, transistor Q_1 can be turned on without incurring switching loss. The circuit naturally causes the transistor turn-on transition to be lossless, and long turn-on switching times can be tolerated. A particularly significant implication of this is that the switching loss associated with reverse recovery of the antiparallel diodes is avoided. Relatively slow diodes, such as the MOSFET body diodes, can be employed for realization of diodes D_1 to D_4. In addition, the output capacitances of transistors Q_1 to Q_4 and diodes D_1 to D_4 do not lead to switching loss.

In general, zero-voltage switching can occur when the resonant tank presents an effective inductive load to the switches, and hence the switch voltage zero crossings occur before the switch current zero crossings. In the bridge configuration, zero-voltage switching is characterized by the half-bridge conduction sequence D_1–Q_1–D_2–Q_2, such that the transistors are turned on while their respective antipar-

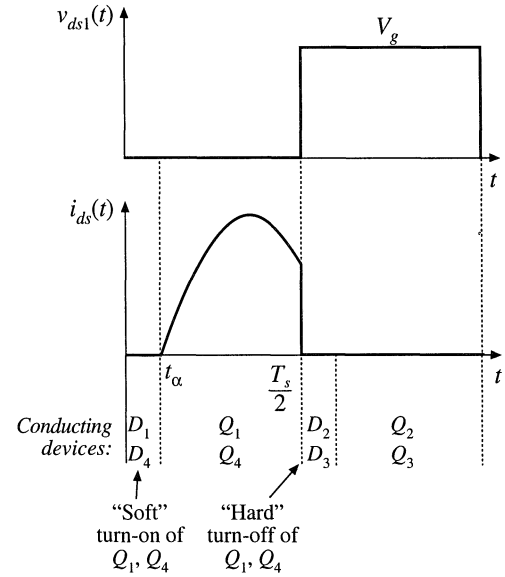

Fig. 19.28 Transistor Q_1 voltage and current waveforms, for operation of the series resonant converter above resonance in the $k = 0$ CCM.

allel diodes conduct. Since the transistor voltage is zero during the entire turn on transition, switching loss due to slow turn-on times or due to energy storage in any of the device capacitances does not occur at turn-on.

The transistor turn-off transition in Fig. 19.28 is similar to that of a PWM switch. In converters that employ IGBTs or other minority-carrier devices, significant switching loss may occur at the turn-off transitions. The current tailing phenomenon causes Q_1 to pass through a period of high instantaneous power dissipation, and switching loss occurs.

To assist the transistor turn off process, small capacitors C_{leg} may be introduced into the legs of the bridge, as demonstrated in Fig. 19.29. In a converter employing MOSFETs, the device output capacitances are sufficient for this purpose, with no need for external discrete capacitors. A delay is also introduced into the gate drive signals, so that there is a short commutation interval when all four transistors are off. During the normal Q_1, D_1, Q_2, and D_2 conduction intervals, the leg capacitors appear in parallel with the semiconductor switches, and have no effect on the converter operation. However, these capacitors introduce commutation intervals at transistor turn-off. When Q_1 is turned off, the tank current $i_s(T_s/2)$ flows through the switch capacitances C_{leg} instead of Q_1, and the voltage across Q_1 and C_{leg} increases. Eventually, the voltage across Q_1 reaches V_g; diode D_2 then becomes forward-biased. If the MOSFET turn-off time is sufficiently fast, then the MOSFET is switched fully off before the drain voltage rises significantly above zero, and negligible turn-off switching loss is incurred. The energy stored in the device capacitances, that is, in C_{leg}, is transferred to the tank inductor. The fact that none of the semiconductor device capacitances or stored charges lead to switching loss is the major advantage of zero-voltage switching, and is the most common motivation for its use. MOSFET converters can typically be operated in this manner, using only the internal drain-to-source capacitances. However, other devices such as IGBTs typically require substantial external capacitances to reduce the losses incurred during the IGBT turn-off transitions.

An additional advantage of zero-voltage switching is the reduction of EMI associated with device capacitances. In conventional PWM converters and also, to some extent, in zero-current switching converters, significant high-frequency ringing and current spikes are generated by the rapid charging and discharging of the semiconductor device capacitances during the turn-on and/or turn-off transitions.

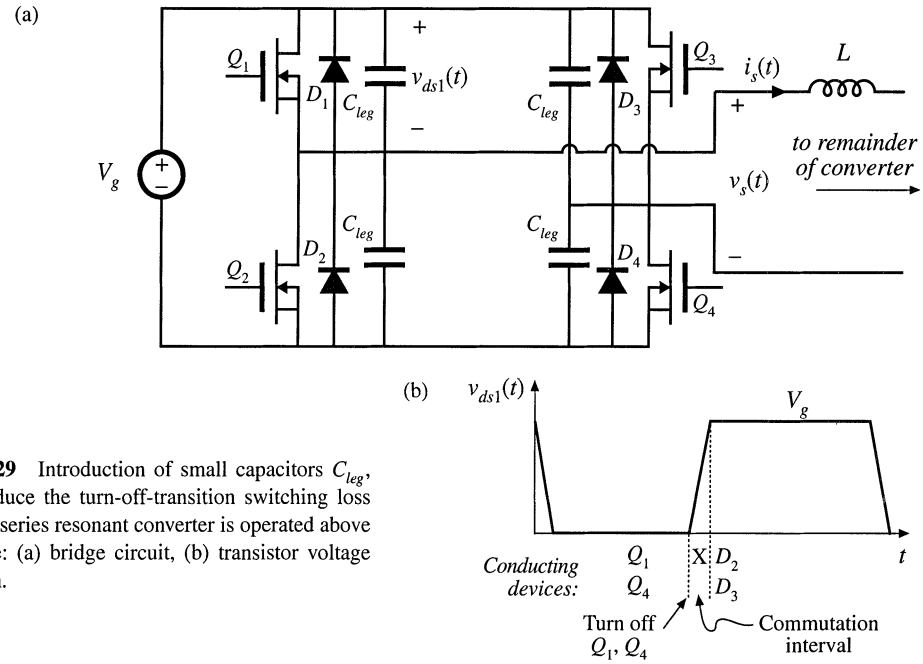

Fig. 19.29 Introduction of small capacitors C_{leg}, which reduce the turn-off-transition switching loss when the series resonant converter is operated above resonance: (a) bridge circuit, (b) transistor voltage waveform.

Ringing is conspicuously absent from the waveforms of converters in which all semiconductor devices switch at zero voltage; these converters inherently do not generate this type of EMI.

19.4 LOAD-DEPENDENT PROPERTIES OF RESONANT CONVERTERS

The properties of the CCM PWM converters studied in previous chapters are largely unaffected by the load current. In consequence, these converters exhibit several desirable properties that are often taken for granted. The transistor current is proportional to the load current; hence conduction losses become small at light load, leading to good light-load efficiency. Also, the output impedance is low, and hence the dc output voltage does not significantly depend on the load i–v characteristic (at least, in CCM). Unfortunately, these good properties are not necessarily shared by resonant converters. Of central importance in design of a resonant converter is the selection of the resonant tank topology and element values, so that the transistor conduction losses at light load are minimized, so that zero-voltage switching is obtained over a wide range of load currents (preferably, for all anticipated loads, but at least at full and intermediate load powers), and so that the converter dynamic range is compatible with the load i–v characteristic. These design issues are addressed in this section.

The conduction loss caused by circulating tank currents is well-recognized as a problem in resonant converter design. These currents are independent of, or only weakly dependent on, the load current, and lead to poor efficiency at light load. In Fig. 19.30, the switch current $i_s(s)$ is equal to $v_s(s)/Z_i(s)$. If we want the switch current to track the load current, then at the switching frequency $\| Z_i \|$ should be dominated by, or at least strongly influenced by, the load resistance R. Unfortunately, this is often not consistent with the requirement for zero-voltage switching, in which Z_i is dominated by a tank inductor.

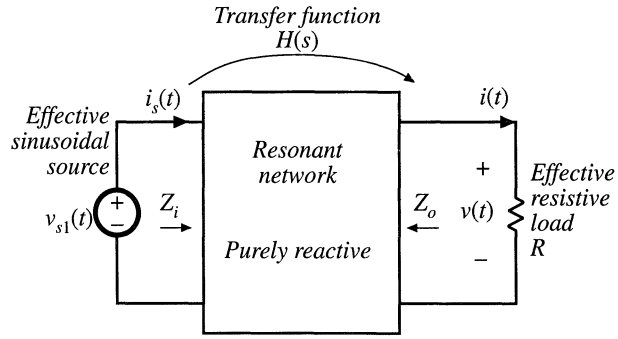

Fig. 19.30 Resonant inverter model.

To design a resonant converter that exhibits good properties, the engineer must develop physical insight into how the load resistance R affects the tank input impedance and output voltage.

In this section, the inverter output characteristics, zero-voltage switching boundary, and the dependence of transistor current on load resistance, are related to the properties of the tank network under the extreme conditions of an open-circuited or short-circuited load. The undamped tank network responses are easily plotted, and the insight needed to optimize the tank network design can be gained quickly.

19.4.1 Inverter Output Characteristics

Let us first investigate how the magnitude of the inverter output voltage $\| v \|$ depends on the load current magnitude $\| i \|$. Consider the resonant inverter system of Fig. 19.30. Let $H_\infty(s)$ be the open-circuit ($R \rightarrow \infty$) transfer function of the tank network:

$$H_\infty(s) = \left. \frac{v(s)}{v_{s1}(s)} \right|_{R \rightarrow \infty} \tag{19.33}$$

and let $Z_{o0}(s)$ be the output impedance, determined when the source $v_{s1}(s)$ is short-circuited. Then we can model the output port of the tank network using the Thevenin-equivalent circuit of Fig. 19.31. Solution of this circuit using the voltage divider formula leads to

$$v(s) = H_\infty(s) v_{s1}(s) \frac{R}{R + Z_{o0}(s)} \tag{19.34}$$

At a given angular switching frequency $\omega_s = 2\pi f_s$, the phasor representing the magnitude and phase of the ac output voltage is found by letting $s = j\omega_s$:

$$v(j\omega_s) = H_\infty(j\omega_s) v_{s1}(j\omega_s) \frac{R}{R + Z_{o0}(j\omega_s)} \tag{19.35}$$

The magnitude can be found by noting that

$$\left\| v(j\omega_s) \right\|^2 = v(j\omega_s) v^*(j\omega_s) \tag{19.36}$$

where $v^*(j\omega_s)$ is the complex conjugate of $v(j\omega_s)$. Substitution of Eq. (19.35) into Eq. (19.36) leads to

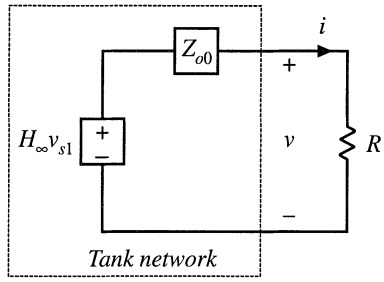

Fig. 19.31 Thevenin-equivalent circuit that models the output port of the tank network.

$$\begin{aligned}\|v(j\omega_s)\|^2 &= \left(H_\infty(j\omega_s)v_{s1}(j\omega_s)\frac{R}{R+Z_{o0}(j\omega_s)}\right)\left(H_\infty(j\omega_s)v_{s1}(j\omega_s)\frac{R}{R+Z_{o0}(j\omega_s)}\right)^* \\ &= H_\infty(j\omega_s)H_\infty^*(j\omega_s)v_{s1}(j\omega_s)v_{s1}^*(j\omega_s)\frac{R^2}{\left(R+Z_{o0}(j\omega_s)\right)\left(R+Z_{o0}(j\omega_s)\right)^*} \\ &= \|H_\infty(j\omega_s)\|^2\|v_{s1}(j\omega_s)\|^2\frac{R^2}{\left(R+Z_{o0}(j\omega_s)\right)\left(R+Z_{o0}(j\omega_s)\right)^*}\end{aligned} \tag{19.37}$$

This result can be further simplified with the assumption that the tank network contains only purely reactive elements, i.e., that any losses or other resistive elements within the tank network have negligible effect. Then the output impedance $Z_{o0}(j\omega_s)$, as well as all other driving-point impedances of the tank network, are purely imaginary quantities. This implies that the complex conjugate $Z_{o0}^*(j\omega_s)$ is given by

$$Z_{o0}^*(j\omega_s) = -Z_{o0}(j\omega_s) \tag{19.38}$$

Substitution of Eq. (19.38) into Eq. (19.37) and simplification leads to

$$\|v(j\omega_s)\|^2 = \frac{\|H_\infty(j\omega_s)\|^2\|v_s(j\omega_s)\|^2}{\left(1+\dfrac{\|Z_{o0}(j\omega_s)\|^2}{R^2}\right)} \tag{19.39}$$

with

$$R = \frac{\|v(j\omega_s)\|}{\|i(j\omega_s)\|} \tag{19.40}$$

Substitution of Eq. (19.40) into Eq. (19.39) and rearrangement of terms yields

$$\|v(j\omega_s)\|^2 + \|i(j\omega_s)\|^2\|Z_{o0}(j\omega_s)\|^2 = \|H_\infty(j\omega_s)\|^2\|v_s(j\omega_s)\|^2 \tag{19.41}$$

Hence, at a given frequency, the inverter output characteristic, that is, the relationship between $\| v(j\omega_s) \|$ and $\| i(j\omega_s) \|$, is elliptical. Equation (19.41) can be further rearranged, into the form

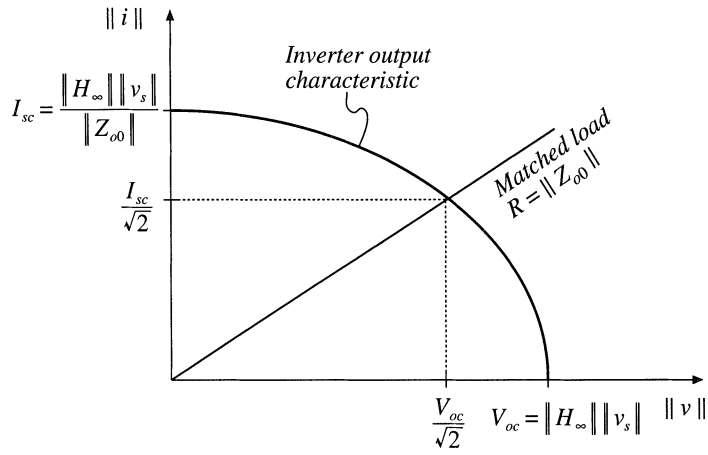

Fig. 19.32 Elliptical output characteristics of resonant inverters. A resistive matched load is also illustrated.

$$\frac{\|v(j\omega_s)\|^2}{V_{oc}^2} + \frac{\|i(j\omega_s)\|^2}{I_{sc}^2} = 1 \tag{19.42}$$

where the open-circuit voltage V_{oc} and short-circuit current I_{sc} are given by

$$\begin{aligned} V_{oc} &= \|H_\infty(j\omega_s)\|\|v_s(j\omega_s)\| \\ I_{sc} &= \frac{\|H_\infty(j\omega_s)\|\|v_s(j\omega_s)\|}{\|Z_{o0}(j\omega_s)\|} = \frac{V_{oc}}{\|Z_{o0}(j\omega_s)\|} \end{aligned} \tag{19.43}$$

These inverter output characteristics are constructed in Fig. 19.32. This characteristic describes how, at a given switching frequency, the ac output voltage magnitude varies as the circuit is loaded. The equilibrium output voltage is given by the intersection of this elliptical characteristic with the load i–v characteristic. For example, Fig. 19.32 also illustrates a superimposed resistive load line having slope $1/R$, in the special case where $R = \| Z_{o0}(j\omega_s) \|$. This value of R corresponds to matched load operation, in which the converter output power is maximized. It can be shown that the operating point is then given by

$$\begin{aligned} \|v(j\omega_s)\|^2 &= \frac{V_{oc}}{\sqrt{2}} \\ \|i(j\omega_s)\|^2 &= \frac{I_{sc}}{\sqrt{2}} \end{aligned} \tag{19.44}$$

Note that Fig. 19.32 can also be applied to the output i–v characteristics of resonant dc–dc converters, since the output rectifier then loads the tank with an effective resistive load R_e.

19.4.2 Dependence of Transistor Current on Load

The transistors must conduct the current appearing at the input port of the tank network, $i_s(t)$. This current is determined by the tank network input impedance $Z_i(j\omega_s)$:

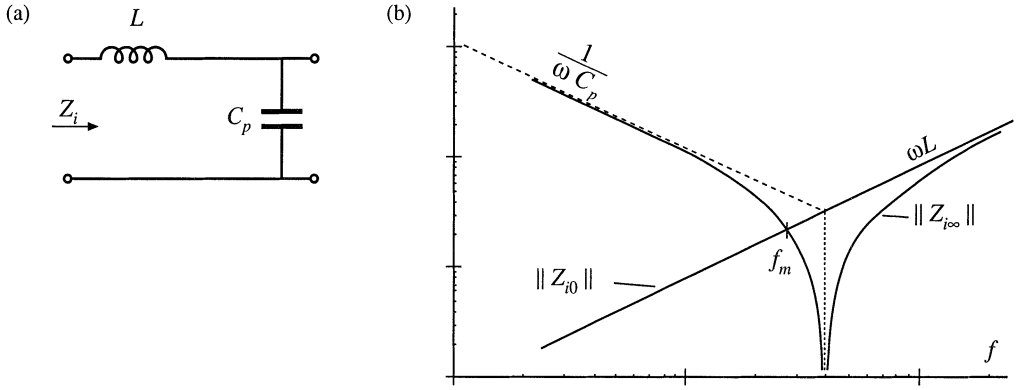

Fig. 19.33 Tank network, parallel resonant converter example: (a) tank circuit, (b) Bode plot of input impedance magnitude $\| Z_i \|$ for the limiting cases $R \to 0$ and $R \to \infty$.

$$i_{s1}(j\omega_s) = \frac{v_{s1}(j\omega_s)}{Z_i(j\omega_s)} \tag{19.45}$$

As described previously, obtaining good light-load efficiency requires that $\| Z_i(j\omega_s) \|$ increase as the load resistance R increases. To understand how $\| Z_i(j\omega_s) \|$ depends on R, let us sketch $\| Z_i(j\omega_s) \|$ in the extreme cases of an open-circuited ($R \to \infty$) and short-circuited ($R \to 0$) load:

$$\begin{aligned} Z_{i0}(j\omega_s) &= Z_i(j\omega_s)\big|_{R \to 0} \\ Z_{i\infty}(j\omega_s) &= Z_i(j\omega_s)\big|_{R \to \infty} \end{aligned} \tag{19.46}$$

For example, consider the parallel resonant converter of Figs. 19.19 to 19.23. The Bode diagrams of the impedances $\| Z_{i0}(j\omega_s) \|$ and $\| Z_{i\infty}(j\omega_s) \|$ are constructed in Fig. 19.33. $Z_{i0}(s)$ is found with the load R shorted, and is equal to the inductor impedance sL. $Z_{i\infty}(s)$, found with the load R open-circuited, is given by the series combination $(sL + 1/sC)$. It can be seen in Fig. 19.33 that the impedance magnitudes $\| Z_{i0}(j\omega_s) \|$ and $\| Z_{i\infty}(j\omega_s) \|$ intersect at frequency f_m. If the switching frequency is chosen such that $f_s < f_m$, then $\| Z_{i\infty}(j\omega_s) \| > \| Z_{i0}(j\omega_s) \|$. The converter then exhibits the desirable characteristic that the no-load switch current magnitude $\| v_s(j\omega_s) \| / \| Z_{i\infty}(j\omega_s) \|$ is smaller than the switch current under short-circuit conditions, $\| v_s(j\omega_s) \| / \| Z_{i0}(j\omega_s) \|$. In fact, the short-circuit switch current is limited by the impedance of the tank inductor, while the open-circuit switch current is determined primarily by the impedance of the tank capacitor.

If the switching frequency is chosen such that $f_s > f_m$, then $\| Z_{i\infty}(j\omega_s) \| < \| Z_{i0}(j\omega_s) \|$. The no-load switch current is then greater in magnitude than the switch current when the load is short-circuited! When the load current is reduced or removed, the transistors will continue to conduct large currents and generate high conduction losses. This causes the efficiency at light load to be poor. It can be concluded that, to obtain good light-load efficiency in the parallel resonant converter, one should choose f_s sufficiently less than f_m. Unfortunately, this requires operation below resonance, leading to reduced output voltage dynamic range and a tendency to lose the zero-voltage switching property.

A remaining question is how $\| Z_i(j\omega_s) \|$ behaves for intermediate values of load between the open-circuit and short-circuit conditions. The answer is given by Theorem 1 below: $\| Z_i(j\omega_s) \|$ varies monotonically with R, and therefore is bounded by $\| Z_{i0}(j\omega_s) \|$ and $\| Z_{i\infty}(j\omega_s) \|$. Hence, the Bode plots of

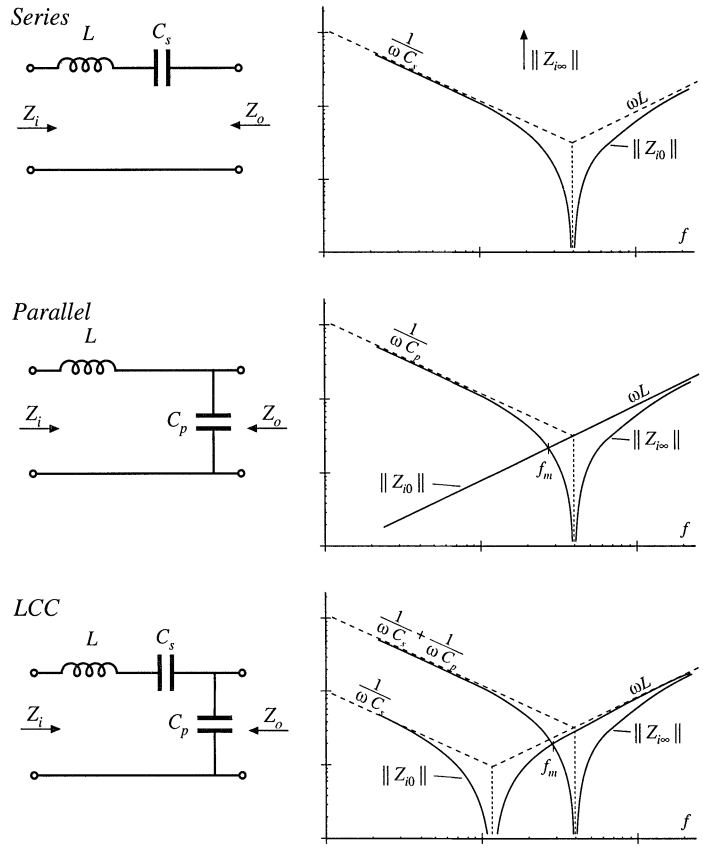

Fig. 19.34 Series, parallel, and LCC resonant tank networks, and their input impedances Z_{i0} and $Z_{i\infty}$.

the limiting cases $\| Z_{i0}(j\omega_s) \|$ and $\| Z_{i\infty}(j\omega_s) \|$ provide a correct qualitative understanding of the behavior of $\| Z_i \|$ for all R. The theorem is valid for lossless tank networks.

***Theorem* 1:** If the tank network is purely reactive, then its input impedance $\| Z_i \|$ is a monotonic function of the load resistance R.

This theorem is proven by use of Middlebrook's Extra Element Theorem (see Appendix C). The tank network input impedance $Z_i(s)$ can be expressed as a function of the load resistance R and the tank network driving-point impedances, as follows:

$$Z_i(s) = Z_{i0}(s) \frac{\left(1 + \frac{R}{Z_{o0}(s)}\right)}{\left(1 + \frac{R}{Z_{o\infty}(s)}\right)} = Z_{i\infty}(s) \frac{\left(1 + \frac{Z_{o0}(s)}{R}\right)}{\left(1 + \frac{Z_{o\infty}(s)}{R}\right)} \tag{19.47}$$

where Z_{i0} and $Z_{i\infty}$ are the resonant network input impedances, with the load short-circuited or open-circuited, respectively, and Z_{o0} and $Z_{o\infty}$ are the resonant network output impedances, with the source input short-circuited or open-circuited, respectively. These terminal impedances are simple functions of the tank elements, and their Bode diagrams are easily constructed. The input impedances of the series reso-

nant, parallel resonant, and LCC inverters are listed in Fig. 19.34. Since these impedances do not depend on the load, they are purely reactive, ideally have zero real parts [38], and their complex conjugates are given by $Z_{o0}{}^{*} = -Z_{o0}$, $Z_{o\infty}{}^{*} = -Z_{o\infty}$, etc. Again, recall that the magnitude of a complex impedance $Z(j\omega)$ can be expressed as the square root of $Z(j\omega)Z^{*}(j\omega)$. Hence, the magnitude of $Z_i(s)$ is given by

$$\begin{aligned} \|Z_i\|^2 = Z_i Z_i^* &= Z_{i0}(s) Z_{i0}^*(s) \frac{\left(1+\dfrac{R}{Z_{o0}(s)}\right)\left(1+\dfrac{R}{Z_{o0}^*(s)}\right)}{\left(1+\dfrac{R}{Z_{o\infty}(s)}\right)\left(1+\dfrac{R}{Z_{o\infty}^*(s)}\right)} \\ &= \|Z_{i0}\|^2 \frac{\left(1+\dfrac{R^2}{\|Z_{o0}\|^2}\right)}{\left(1+\dfrac{R^2}{\|Z_{o\infty}\|^2}\right)} \end{aligned} \tag{19.48}$$

where Z_i^{*} is the complex conjugate of Z_i.
Next, let us differentiate Eq. (19.48) with respect to R:

$$\frac{d\|Z_i\|^2}{dR} = 2R\|Z_{i0}\|^2 \frac{\left(\dfrac{1}{\|Z_{o0}\|^2} - \dfrac{1}{\|Z_{o\infty}\|^2}\right)}{\left(1+\dfrac{R^2}{\|Z_{o\infty}\|^2}\right)^2} \tag{19.49}$$

The derivative has roots at (*i*) $R = 0$, (*ii*) $R = \infty$, and in the special case (*iii*) where $\| Z_{i0} \| = \| Z_{i\infty} \|$. Since the derivative is otherwise nonzero, the resonant network input impedance $\| Z_i \|$ is a monotonic function of R, over the range $0 < R < \infty$. In special case (*iii*), $\| Z_i \|$ is independent of R. Therefore, Theorem 1 is proved.

An example is given in Figs. 19.36 and 19.35, for the LCC inverter. Figure 19.35 illustrates the impedance asymptotes of the limiting cases $\| Z_{i0} \|$ and $\| Z_{i\infty} \|$. Variation of $\| Z_i \|$ between these limits, for finite nonzero R, is illustrated in Fig. 19.36. The open-circuit resonant frequency f_∞ and the short-circuit resonant frequency f_0 are given by

$$\begin{aligned} f_0 &= \frac{1}{2\pi\sqrt{LC_s}} \\ f_\infty &= \frac{1}{2\pi\sqrt{L\, C_s \| C_p}} \end{aligned} \tag{19.50}$$

where $C_s \| C_p$ denotes inverse addition of C_s and C_p:

$$C_s \| C_p = \frac{1}{\dfrac{1}{C_s} + \dfrac{1}{C_p}} \tag{19.51}$$

For the LCC inverter, the impedance magnitudes $\| Z_{i0} \|$ and $\| Z_{i\infty} \|$ are equal at frequency f_m, given by

$$f_m = \frac{1}{2\pi\sqrt{L\, C_s \| 2C_p}} \tag{19.52}$$

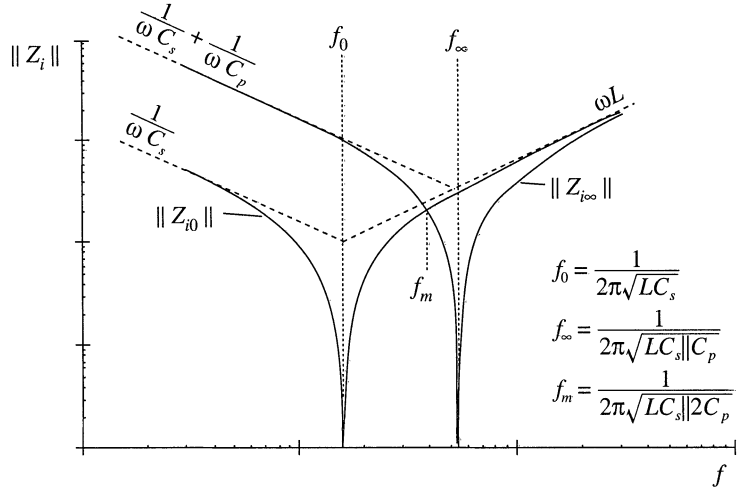

Fig. 19.35 Construction of the quantities $\| Z_{i0} \|$ and $\| Z_{i\infty} \|$, for the LCC inverter.

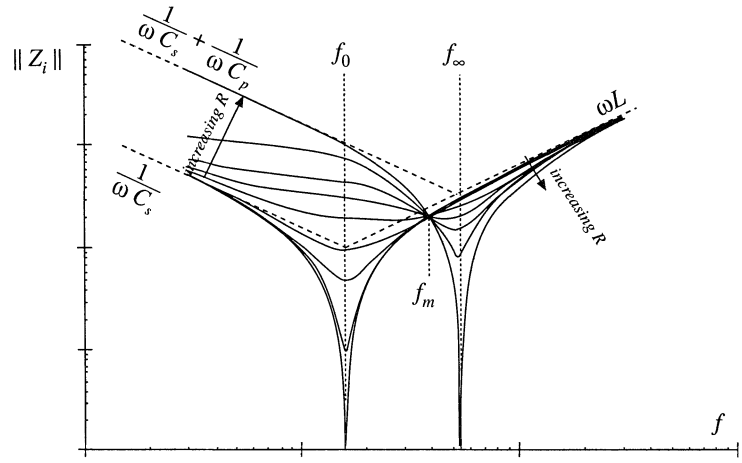

Fig. 19.36 Variation of tank network input impedance $\| Z_i \|$ with load resistance R, LCC inverter. As the load resistance is increased, $\| Z_i \|$ changes monotonically from $\| Z_{i0} \|$ to $\| Z_{i\infty} \|$.

If the switching frequency is chosen to be greater than f_m, then $\| Z_{i\infty} \|$ is less than $\| Z_{i0} \|$. This implies that, as the load current is decreased, the transistor current will increase. Such a converter will have poor efficiency at light load, and will exhibit significant circulating currents. If the switching frequency is chosen to be less than f_m, then the transistor current will increase with decrease with decreasing load current. The short-circuit current is limited by $\| Z_{i0} \|$, while the circulating currents under open-circuit conditions are determined by $\| Z_{i\infty} \|$. In general, if $f > f_m$, then the transistor current is greater than or equal to the short-circuit current for all R. The inequality is reversed when $f < f_m$.

The impedance magnitudes $\| Z_{i0} \|$ and $\| Z_{i\infty} \|$ are illustrated in Fig. 19.34 for the series, parallel, and LCC tank networks. In the case of the series tank network, $\| Z_{i\infty} \| = \infty$. In consequence, the no-load transistor current is zero, both above resonance and below resonance. Hence, the series resonant inverter exhibits the desirable property that the transistor current is proportional to the load current. In addition, when the load is short-circuited, the current magnitude is limited by the impedance of the series resonant tank. For the parallel and LCC inverters, it is desirable to operate below the frequency f_m.

Thus, the dependence of the transistor current on load can be easily determined, using an intuitive frequency-domain approach.

19.4.3 Dependence of the ZVS/ZCS Boundary on Load Resistance

It is also necessary to determine the critical load resistance $R = R_{crit}$ at the boundary between ZVS and ZCS. This boundary can also be expressed as a function of the impedances Z_{i0} and $Z_{i\infty}$.

As discussed in Section 19.3, zero-voltage switching occurs when the switch current $i_s(t)$ lags the switch voltage $v_s(t)$. Zero-voltage switching occurs when $i_s(t)$ leads $v_s(t)$. This definition ignores the effects of semiconductor output capacitances, and hence gives an approximate ZVS/ZCS boundary. The phase between the switch current and switch voltage is again determined by the input impedance of the tank network:

$$i_{s1}(j\omega_s) = \frac{v_{s1}(j\omega_s)}{Z_i(j\omega_s)} \tag{19.53}$$

Hence, zero-voltage switching occurs when $Z_i(j\omega_s)$ is inductive in nature, zero-current switching occurs when $Z_i(j\omega_s)$ is capacitive in nature, and the ZVS/ZCS boundary occurs where $Z_i(j\omega_s)$ has zero phase.

It is instructive to again consider the limiting cases of a short-circuited and open-circuited load. The Bode plots of $Z_{i0}(j\omega_s)$ and $Z_{i\infty}(j\omega_s)$ for an LCC inverter example are sketched in Fig. 19.37. Since, in these limiting cases, the input impedance Z_i is composed only of the reactive tank elements, $Z_{i0}(j\omega_s)$ and $Z_{i\infty}(j\omega_s)$ are purely imaginary quantities having phase of either – 90° or + 90°. For $f_s < f_0$, both $Z_{i0}(j\omega_s)$ and $Z_{i\infty}(j\omega_s)$ are dominated by the tank capacitor or capacitors; the phase of $Z_i(j\omega_s)$ is therefore – 90°. Hence, zero-current switching is obtained under both short-circuit and open-circuit conditions. For $f_s > f_\infty$, both $Z_{i0}(j\omega_s)$ and $Z_{i\infty}(j\omega_s)$ are dominated by the tank inductor; hence the phase of $Z_i(j\omega_s)$ is + 90°. Zero-voltage switching is obtained for both a short-circuited and an open-circuited load. For $f_0 < f_s < f_\infty$, $Z_{i0}(j\omega_s)$ is dominated by the tank inductor while $Z_{i\infty}(j\omega_s)$ is dominated by the tank capacitors. This implies that zero-voltage switching is obtained under short-circuit conditions, and zero-voltage switching is obtained under open-circuit conditions. For this case, there must be some critical value of load resistance $R = R_{crit}$ that represents the boundary between ZVS and ZCS, and that causes the phase of $Z_i(j\omega_s)$ to be equal to 0°.

The behavior of $Z_i(j\omega_s)$ for nonzero finite R is easily extrapolated from the limiting cases dis-

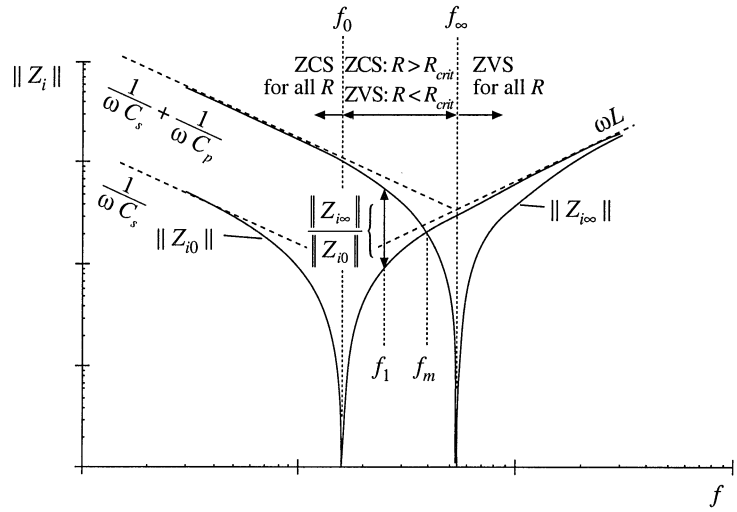

Fig. 19.37 Use of the input impedance quantities Z_{i0} and $Z_{i\infty}$ to determine the ZCS/ZVS boundaries, LCC example.

cussed above. Theorem 2 below shows that:

1. If zero-current switching occurs for both an open-circuited load and a short-circuited load [i.e., $Z_{i0}(j\omega_s)$ and $Z_{i\infty}(j\omega_s)$ both have phase + 90°], then zero-current switching occurs for all loads.
2. If zero-voltage switching occurs for both an open-circuited load and a short-circuited load [i.e., $Z_{i0}(j\omega_s)$ and $Z_{i\infty}(j\omega_s)$ both have phase – 90°], then zero-voltage switching occurs for all loads.
3. If zero-voltage switching occurs for an open-circuited load and zero-current switching occurs for a short-circuited load [i.e., $Z_{i0}(j\omega_s)$ has phase – 90° and $Z_{i\infty}(j\omega_s)$ has phase + 90°], then zero-voltage switching occurs for $R > R_{crit}$, and zero-current switching occurs for $R < R_{crit}$, with R_{crit} given by Eq. (19.54) below.
4. If zero-current switching occurs for an open-circuited load and zero-voltage switching occurs for a short-circuited load [i.e., $Z_{i0}(j\omega_s)$ has phase + 90° and $Z_{i\infty}(j\omega_s)$ has phase – 90°], then zero-current switching occurs for $R > R_{crit}$, and zero-voltage switching occurs for $R < R_{crit}$, with R_{crit} given by Eq. (19.54) below.

For the LCC example, we can therefore conclude that, for $f_s < f_0$, zero-current switching occurs for all values of R. For $f_s > f_\infty$, zero-voltage switching occurs for all values of R. For $f_0 < f_s < f_\infty$, the boundary between ZVS and ZCS is given by Eq. (19.54).

***Theorem* 2:** If the tank network is purely reactive, then the boundary between zero-current switching and zero-voltage switching occurs when the load resistance R is equal to the critical value R_{crit}, given by

$$R_{crit} = \| Z_{o0} \| \sqrt{\frac{-Z_{i\infty}}{Z_{i0}}} \tag{19.54}$$

This theorem relies on the assumption that zero-current switching occurs when the tank input impedance is capacitive in nature, while zero-voltage switching occurs for inductive input impedances. The boundary therefore occurs where the phase of $Z_i(j\omega)$ is zero. This definition gives a necessary but not sufficient condition for zero-voltage switching when significant semiconductor output capacitance is present.

The result is derived by finding the value of R which causes the imaginary part of $Z_i(j\omega)$ in Eq. (19.47) to be zero. Since the tank network is assumed to ideal and lossless, the impedances $Z_{o\infty}$, Z_{o0}, and $Z_{i\infty}$ must have zero real parts. Hence,

$$\mathrm{Im}\left(Z_i(R_{crit})\right) = \mathrm{Im}\left(Z_{i\infty}\right) \mathrm{Re}\left(\frac{1 + \dfrac{Z_{o0}}{R_{crit}}}{1 + \dfrac{Z_{o\infty}}{R_{crit}}} \right) = \mathrm{Im}\left(Z_{i\infty}\right) \frac{\left(1 - \dfrac{Z_{o0} Z_{o\infty}}{R_{crit}^2} \right)}{\left(1 + \dfrac{\| Z_{o\infty} \|^2}{R_{crit}^2} \right)} = 0 \tag{19.55}$$

where Im(Z) and Re(Z) denote the imaginary and real parts of the complex quantity Z. The nontrivial solution to Eq. (19.55) is given by

$$1 = \frac{Z_{o0} Z_{o\infty}}{R_{crit}^2} \tag{19.56}$$

hence,

$$R_{crit} = \sqrt{Z_{o0} Z_{o\infty}} \tag{19.57}$$

A useful equivalent form makes use of the reciprocity identities

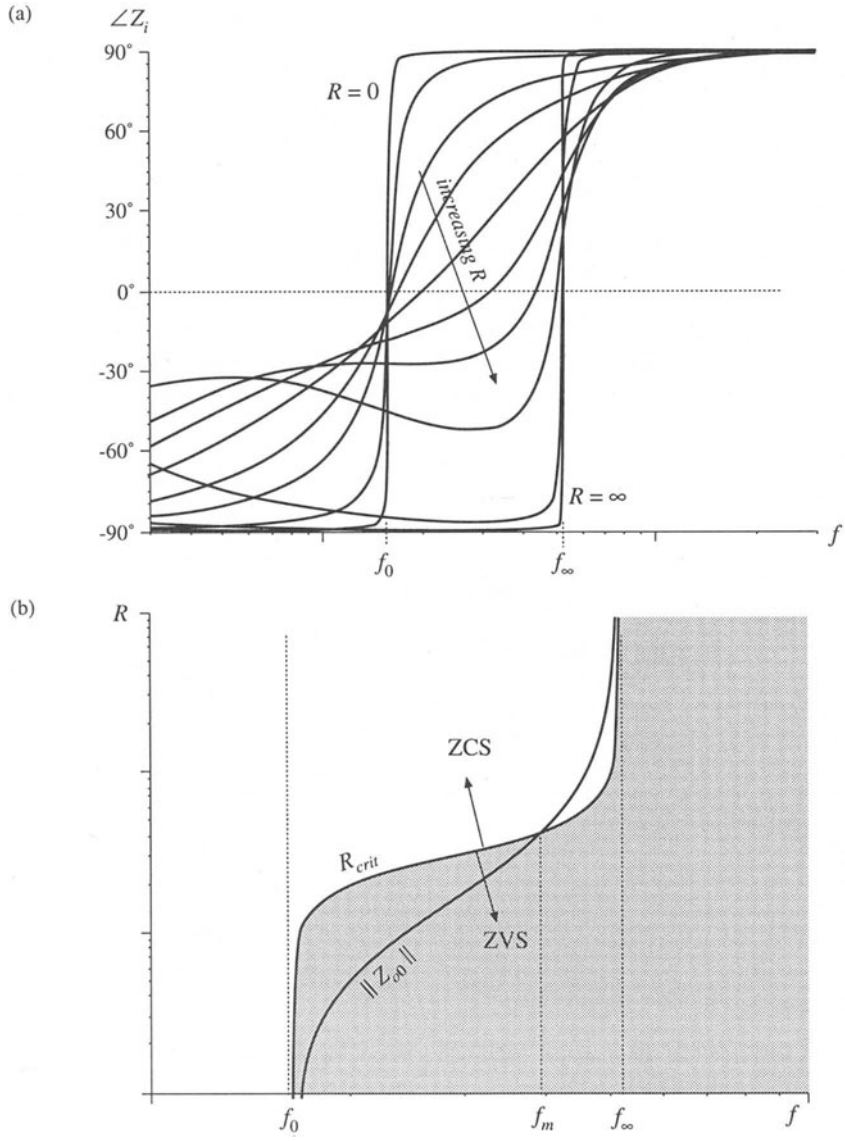

Fig. 19.38 ZCS/ZVS boundary, LCC inverter example: (a) variation of tank network input impedance phase shift with load resistance, (b) Comparison of R_{crit} with matched-load impedance $\| Z_{o0} \|$.

$$\frac{Z_{o0}}{Z_{o\infty}} = \frac{Z_{i0}}{Z_{i\infty}} \tag{19.58}$$

Use of Eq. (19.58) to eliminate $Z_{o\infty}$ from Eq. (19.57) leads to

$$R_{crit} = \| Z_{o0} \| \sqrt{\frac{-Z_{i\infty}}{Z_{i0}}} \tag{19.59}$$

This is the desired result. The quantity Z_{o0} is the inverter output impedance, and $R = \| Z_{o0} \|$ corresponds to operation at matched load with maximum output power. The impedances $Z_{i\infty}$ and Z_{i0} are purely imaginary, and hence Eq. (19.59) has no real solution unless $Z_{i\infty}$ and Z_{i0} are of opposite phase. As illustrated in Fig. 19.37, if at a given frequency $Z_{i\infty}$ and Z_{i0} are both inductive, then zero-voltage switching occurs for all loads. Zero-current switching occurs for all loads when $Z_{i\infty}$ and Z_{i0} are both capacitive. Therefore, Theorem 2 is proved.

Figure 19.38(a) illustrates the phase response of $Z_i(j\omega)$ as R varies from 0 to ∞, for the LCC inverter. A typical dependence of R_{crit} and the matched-load impedance $\| Z_{o0} \|$ on frequency is illustrated in Fig. 19.38(b). Zero-voltage switching occurs for all loads when $f > f_\infty$, and zero-current switching occurs for all loads when $f < f_0$. Over the range $f_0 < f < f_\infty$, Z_{i0} is inductive while $Z_{i\infty}$ is capacitive; hence, zero-voltage switching occurs for $R < R_{crit}$ while zero-current switching occurs for $R > R_{crit}$. At frequency f_m, $R_{crit} = \| Z_{o0} \|$, and hence the ZVS/ZCS boundary is encountered exactly at matched load. It is commonly desired to obtain zero-voltage switching at matched load, with low circulating currents and good efficiency at light load. It is apparent that this requires operation in the range $f_0 < f < f_m$. Zero-voltage switching will then be obtained under matched-load and short-circuit conditions, but will be lost at light load. The choice of element values such that $\| Z_{i0} \| \ll \| Z_{i\infty} \|$ is advantageous in that the range of loads leading to zero-voltage switching is maximized.

19.4.4 Another Example

As a final example, let us consider selection of the resonant tank elements to obtain a given output characteristic at a certain switching frequency, and let's evaluate the effect of this choice on R_{crit}. It is desired to operate a resonant inverter at switching frequency f_s = 100 kHz, with an input voltage of V_g = 160 V. The converter should be capable of producing an open-circuit peak output voltage V_{oc} = 400 V, and should also produce a nominal output of 150 Vrms at 25 W. It is desired to select resonant tank elements that accomplish this.

The specifications imply that the converter should exhibit an open-circuit transfer function of

$$\left\| H_\infty(j\omega_s) \right\| = \frac{V_{oc}}{V_{s1}} = \frac{(400\text{ V})}{\left(\frac{4}{\pi} 160\text{ V}\right)} = 1.96 \tag{19.60}$$

The required short-circuit current is found by solving Eq. (19.42) for I_{sc}:

$$I_{sc} = \frac{I}{\sqrt{1 - \left(\frac{V}{V_{oc}}\right)^2}} \tag{19.61}$$

The specifications also imply that the peak voltage and current at the nominal operating point are

$$
\begin{aligned}
V &= 150\sqrt{2} = 212\ \text{V} \\
I &= \frac{P}{V_{rms}}\sqrt{2} = \frac{25\ \text{W}}{150\ \text{V}}\sqrt{2} = 0.236\ \text{A} \\
R_{nom} &= \frac{V}{I} = 900\ \Omega
\end{aligned}
\tag{19.62}
$$

Substitution of Eq. (19.62) into Eq. (19.61) yields

$$
I_{sc} = \frac{(0.236\ \text{A})}{\sqrt{1 - \left(\frac{212\ \text{V}}{400\ \text{V}}\right)^2}} = 0.278\ \text{A}
\tag{19.63}
$$

Matched load therefore occurs at the operating point

$$
\begin{aligned}
V_{mat} &= \frac{V_{oc}}{\sqrt{2}} = 283\ \text{V} \\
I_{mat} &= \frac{I_{sc}}{\sqrt{2}} = 0.196\ \text{A} \\
\left\| Z_{o0}(j\omega_s) \right\| &= \frac{V_{oc}}{I_{sc}} = 1439\ \Omega
\end{aligned}
\tag{19.64}
$$

Let us select the values of the tank elements in the LCC tank network illustrated in Fig. 19.39(a). The impedances of the series and parallel branches can be represented using the reactances X_s and X_p illustrated in Fig. 19.39(b), with

$$
\begin{aligned}
jX_s &= j\omega_s L + \frac{1}{j\omega_s C_s} = j\left(\omega_s L - \frac{1}{\omega_s C_s}\right) \\
jX_p &= \frac{1}{j\omega_s C_p} = j\left(-\frac{1}{\omega_s C_p}\right)
\end{aligned}
\tag{19.65}
$$

The transfer function $H_\infty(j\omega_s)$ is given by the voltage divider formula

$$
H_\infty(j\omega_s) = \frac{jX_p}{jX_s + jX_p}
\tag{19.66}
$$

The output impedance $Z_{o0}(j\omega_s)$ is given by the parallel combination

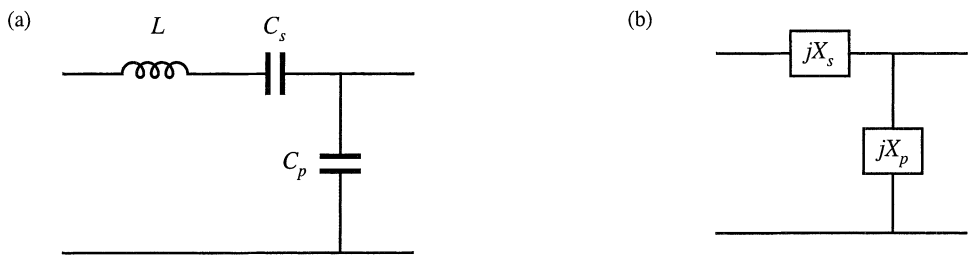

Fig. 19.39 Tank network of the LCC inverter example: (a) schematic, (b) representation of series and parallel branches by reactances X_s and X_p.

$$Z_{o0}(j\omega_s) = jX_s \| jX_p = \frac{-X_s X_p}{j(X_s + X_p)} \tag{19.67}$$

Solution of Eqs. (19.66) and (19.67) for X_p and X_s leads to

$$\begin{aligned} jX_p &= \frac{Z_{o0}(j\omega_s)}{1 - H_\infty(j\omega_s)} \\ X_s &= X_p \frac{1 - H_\infty(j\omega_s)}{H_\infty(j\omega_s)} \end{aligned} \tag{19.68}$$

Hence, the capacitance C_p should be chosen equal to

$$\begin{aligned} X_p &= -1499\ \Omega \\ C_p &= -\frac{1}{\omega_s X_p} = \frac{H_\infty(j\omega_s) - 1}{\omega_s \| Z_{o0}(j\omega_s) \|} = \frac{(1.96) - 1}{(2\pi\ 100\ \text{kHz})(1439\ \Omega)} \cong 1\ \text{nF} \end{aligned} \tag{19.69}$$

and the reactance of the series branch should be chosen according to

$$X_s = X_p \frac{1 - H_\infty(j\omega_s)}{H_\infty(j\omega_s)} = (-1493\ \Omega)\frac{1 - (1.96)}{(1.96)} = 733\ \Omega \tag{19.70}$$

Since X_s is comprised of the series combination of the inductor L and capacitor C_s, there is a degree of freedom in choosing the values of L and capacitor C_s to realize X_s. For example, we could choose C_s very large (tending to a short circuit); this effectively would result in a parallel resonant converter with $L = X_s/\omega_s = 1.17$ mH. For nonzero C_s, L must be chosen according to

$$L = \frac{1}{\omega_s}\left(X_s + \frac{1}{\omega_s C_s}\right) \tag{19.71}$$

For example, the choice $C_s = C_p = 1.06$ nF leads to $L = 3.5$ mH. Designs using different C_s will exhibit exactly the same characteristics at the design frequency; however, the behavior at other switching frequencies will differ.

For the tank network illustrated in Fig. 19.39, the value of R_{crit} is completely determined by the parameters of the output characteristic ellipse; i.e., by the specification of V_g, V_{oc} and I_{sc}. Note that $Z_{o\infty}$, the tank output impedance with the tank input port open-circuited, is equal to jX_p. Substitution of expressions for $Z_{o\infty}$ and Z_{o0} into Eq. (19.57) leads to the following expression for R_{crit}:

$$R_{crit} = \sqrt{\frac{Z_{o0}^2(j\omega_s)}{1 - H_\infty(j\omega_s)}} \tag{19.72}$$

Since Z_{o0} and H_∞ are determined by the operating point specifications, then R_{crit} is also. Evaluation of Eq. (19.72) for this example leads to $R_{crit} = 1466\ \Omega$. Therefore, the inverter will operate with zero-voltage switching for $R < 1466\ \Omega$, including at the nominal operating point $R = 900\ \Omega$. Other topologies of tank network, more complex than the circuit illustrated in Fig. 19.39(b), may have additional degrees of freedom that allow R_{crit} to be independently chosen.

The choice $C_s = 3C_p = 3.2$ nF leads to L = 1.96 μH. The following frequencies are obtained:

$$\begin{aligned} f_\infty &= 127 \text{ kHz} \\ f_m &= 100.6 \text{ kHz} \\ f_s &= 100.0 \text{ kHz} \\ f_0 &= 64 \text{ kHz} \end{aligned} \tag{19.73}$$

Regardless of how C_s is chosen, the open-circuit tank input impedance is

$$Z_{i\infty} = j\left(X_s + X_p\right) = j\left(733\ \Omega + (-1493\ \Omega)\right) = -j760\ \Omega \tag{19.74}$$

Therefore, when the load is open-circuited, the transistor peak current has magnitude

$$I_{s1} = \frac{V_{s1}}{\left\| Z_{i\infty} \right\|} = \frac{\frac{4}{\pi}\left(160 \text{ V}\right)}{760\ \Omega} = 0.268 \text{ A} \tag{19.75}$$

When the load is short-circuited, the transistor peak current has magnitude

$$I_{s1} = \frac{V_{s1}}{\left\| Z_{i0} \right\|} = \frac{V_{s1}}{\left| X_s \right|} = \frac{\frac{4}{\pi}\left(160 \text{ V}\right)}{\left(733\ \Omega\right)} = 0.278 \text{ A} \tag{19.76}$$

which is nearly the same as the result in Eq. (19.75). The somewhat large open-circuit switch current occurs because of the relatively-high specified open-circuit output voltage; lower values of V_{oc} would reduce the result in Eq. (19.75).

19.5 EXACT CHARACTERISTICS OF THE SERIES AND PARALLEL RESONANT CONVERTERS

The exact steady-state behavior of resonant converters can be determined via methods such as state-plane analysis. A detailed analysis of resonant dc–dc converters is beyond the scope of this book. However, the exact steady-state characteristics of ideal series [1, 13–20] and parallel [6, 22–25] resonant dc–dc converters (Fig. 19.40) are summarized in this section. Small-signal ac modeling has also been described in the literature; several relevant papers are [27–30].

19.5.1 Series Resonant Converter

At a given switching frequency, the series resonant dc–dc converter can operate in one continuous conduction mode, and possibly in several discontinuous conduction modes. The mode index k is defined as the integer that satisfies

$$\frac{f_0}{k+1} < f_s < \frac{f_0}{k} \quad \text{or} \quad \frac{1}{k+1} < F < \frac{1}{k} \tag{19.77}$$

where $F = f_s/f_0$ is the normalized switching frequency. The subharmonic number ξ is defined as

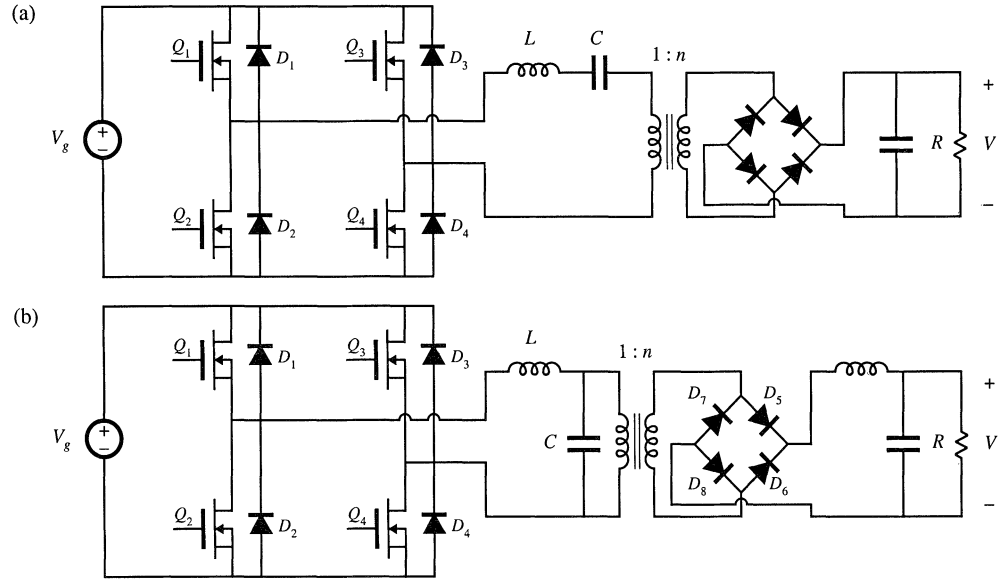

Fig. 19.40 Transformer-isolated resonant dc–dc converters: (a) series resonant converter, (b) parallel resonant converter.

$$\xi = k + \frac{1 + (-1)^k}{2} \tag{19.78}$$

Values of k and ξ as functions of f_s are summarized in Fig. 19.41(a). The subharmonic number ξ denotes the dominant harmonic that excites the tank resonance. When the converter is heavily loaded, it operates in type k continuous conduction mode. As the load is reduced (i.e., as the load resistance R is increased), the converter enters the type k discontinuous conduction mode. Further reducing the load causes the converter to enter the type $(k-1)$ DCM, type $(k-2)$ DCM,..., type 1 DCM. There is no type 0 DCM, and hence when the converter operates above resonance, only the type 0 continuous conduction mode is possible.

In the type k continuous conduction mode, the series resonant converter exhibits elliptical output characteristics, given by

$$M^2\xi^2 \sin^2\left(\frac{\gamma}{2}\right) + \frac{1}{\xi^2}\left(\frac{J\gamma}{2} + (-1)^k\right)^2 \cos^2\left(\frac{\gamma}{2}\right) = 1 \tag{19.79}$$

For the transformer-isolated converters of Fig. 19.40, M and J are related to the load voltage V and load current I according to

$$M = \frac{V}{nV_g} \qquad J = \frac{InR_0}{V_g} \tag{19.80}$$

Again, R_0 is the tank characteristic impedance, referred to the transformer primary side. The quantity γ is the angular length of one-half of the switching period:

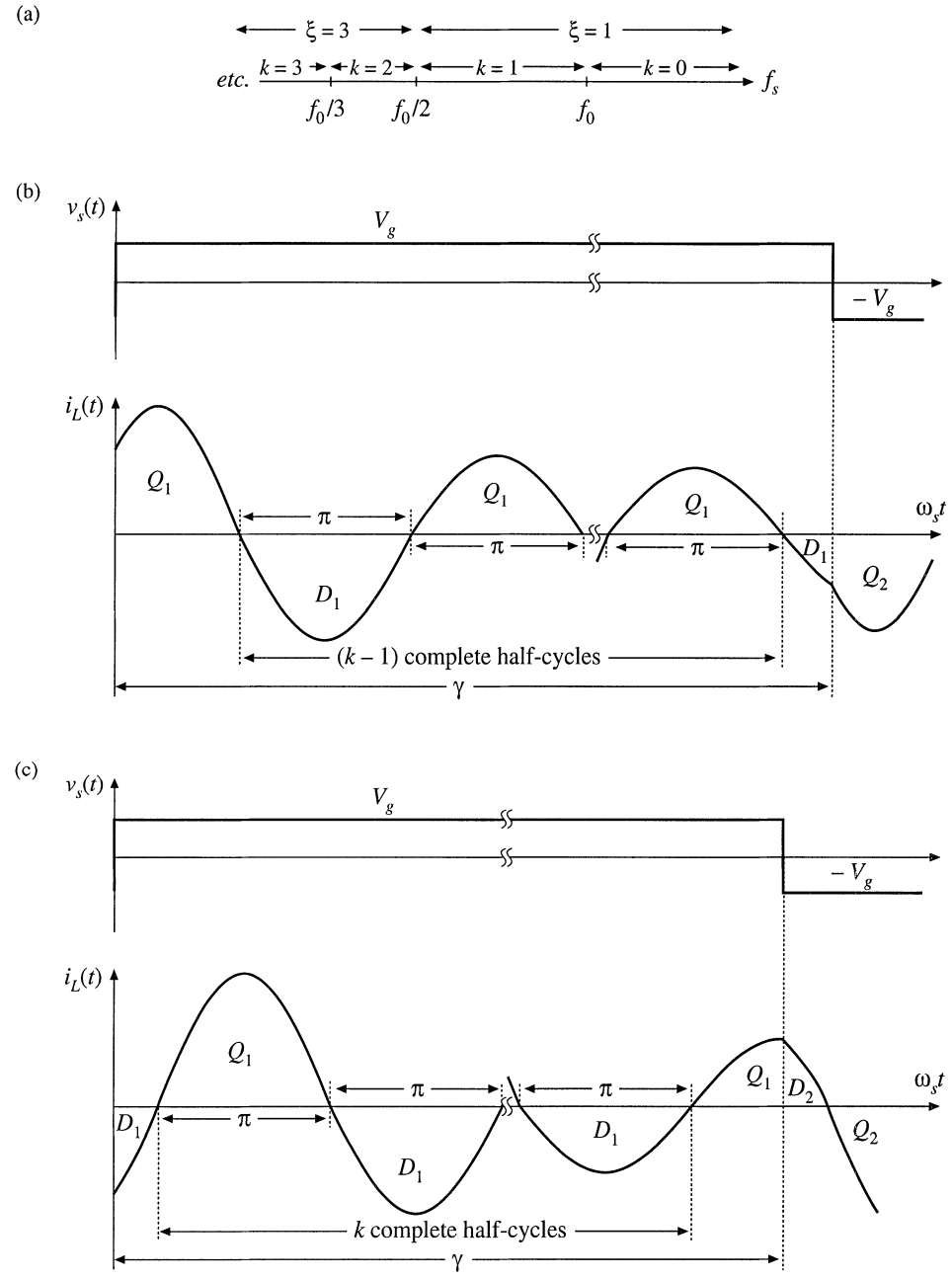

Fig. 19.41 Continuous conduction modes of the series resonant converter: (a) switching frequency ranges over which various mode indices k and subharmonic numbers ξ occur; (b) tank inductor current waveform, type k CCM, for odd k; (c) tank inductor current waveform, type k CCM, for even k.

$$\gamma = \frac{\omega_0 T_s}{2} = \frac{\pi}{F} \tag{19.81}$$

Equation (19.79) is valid only for k satisfying Eq. (19.77). It predicts that the voltage conversion ratio M is restricted to the range

$$0 \le M \le \frac{1}{\xi} \tag{19.82}$$

This is consistent with Eq. (19.21).

Typical CCM tank current waveforms are illustrated in Fig. 19.41. When k is even, the tank inductor current is initially negative. In consequence, the switch network antiparallel diodes conduct first, for a fraction of a half resonant cycle. If k is odd, then each half switching period is initiated by conduction of the switch network transistors. In either case, this is followed by $(\xi - 1)$ complete tank half-cycles of ringing. The half-switching period is then concluded by a subinterval shorter than one complete resonant half-cycle, in which the device that did not initially conduct is on. The next half switching period then begins, and is symmetrical.

The steady-state control-plane characteristic can be found for a resistive load R obeying $V = IR$, by substitution of the normalized relation $J = MQ$ into Eq. (19.79), where $Q = n^2 R_0/R$. Use of the quadratic formula and some algebraic manipulations allows solution for M, as a function of load (via Q) and switching frequency (via γ):

$$M = \frac{\left(\frac{Q\gamma}{2}\right)}{\xi^4 \tan^2\left(\frac{\gamma}{2}\right) + \left(\frac{Q\gamma}{2}\right)^2} \left[(-1)^{k+1} + \sqrt{1 + \frac{\left[\xi^2 - \cos^2\left(\frac{\gamma}{2}\right)\right]\left[\xi^4 \tan^2\left(\frac{\gamma}{2}\right) + \left(\frac{Q\gamma}{2}\right)^2\right]}{\left(\frac{Q\gamma}{2}\right)^2 \cos^2\left(\frac{\gamma}{2}\right)}} \right] \tag{19.83}$$

This is the closed-form relationship between the conversion ratio M and the switching frequency, for a resistive load. It is valid for any continuous conduction mode k.

The type k discontinuous conduction modes, for k odd, occur over the frequency range

$$f_s < \frac{f_0}{k} \tag{19.84}$$

In these modes, the output voltage is independent of both load current and switching frequency, and is described by

$$M = \frac{1}{k} \tag{19.85}$$

The type k discontinuous conduction mode, for odd k, occurs over the range of load currents given by

$$\frac{2(k+1)}{\gamma} > J > \frac{2(k-1)}{\gamma} \tag{19.86}$$

In the odd discontinuous conduction modes, the tank current rings for k complete resonant half cycles. All four output bridge rectifier diodes then become reverse-biased, and the tank current remains at zero until the next switching half-period begins, as illustrated in Fig. 19.42. Series resonant converters are not

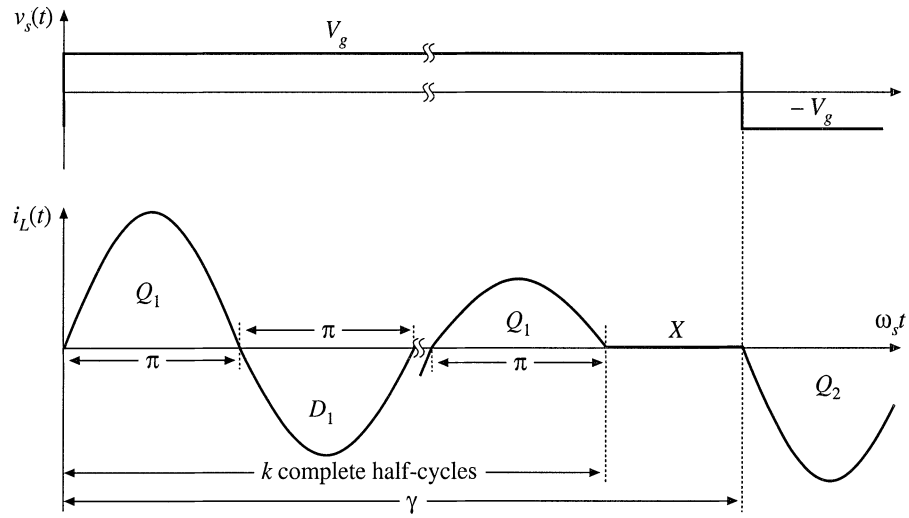

Fig. 19.42 Tank inductor current waveform, type k DCM, for odd k.

normally purposely designed to operate in odd discontinuous conduction modes, because the output voltage is not controllable. Nonetheless, when the load is removed with $f_s < f_0$, the series resonant converter operates in $k = 1$ DCM with $M = 1$.

The type k discontinuous conduction mode, for k even, also occurs over the frequency range

$$f_s < \frac{f_0}{k} \tag{19.87}$$

Even discontinuous conduction modes exhibit current source characteristics, in which the load current is a function of switching frequency and input voltage, but not of the load voltage. The output relationship is:

$$J = \frac{2k}{\gamma} \tag{19.88}$$

Operation in this mode occurs for

$$\frac{1}{k-1} > M > \frac{1}{k+1} \tag{19.89}$$

In the even discontinuous conduction modes, the tank current rings for k complete resonant half-cycles during each switching half-period. All four output bridge then become reverse-biased, and the tank current remains at zero until the next switching half-period is initiated. Tank current waveforms are illustrated in Fig. 19.43 for even DCM.

The series resonant converter possesses some unusual properties when operated in an even discontinuous conduction mode. A dc equivalent circuit is given in Fig. 19.44, consisting of a gyrator with gyration conductance $g = 2k/gn^2R_0$. The gyrator has the property of transforming circuits into their dual networks; in the typical dc–dc converter application, the input voltage source V_g is effectively transformed into its dual, an output current source of value gV_g. Series resonant converters have been purposely designed to operate in the $k = 2$ DCM, at power levels of several tens of kW.

The complete control plane characteristics can now be plotted using Eqs. (19.77) to (19.89).

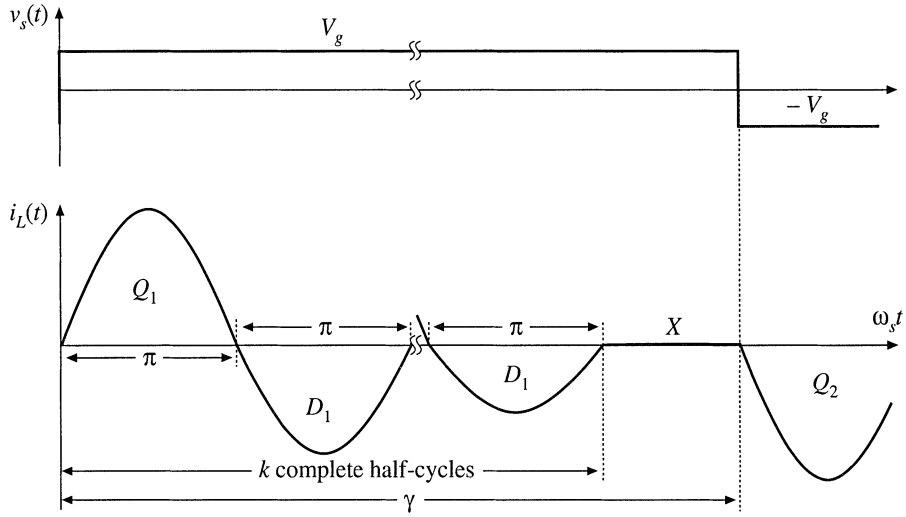

Fig. 19.43 Tank inductor current waveform, type k DCM, for even k.

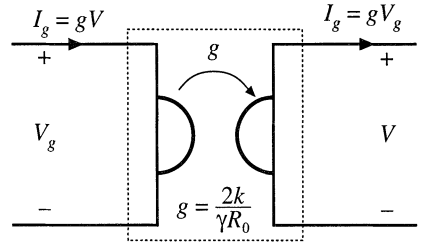

Fig. 19.44 Steady-state equivalent circuit model for an even discontinuous conduction mode: an effective gyrator. The converter exhibits current source characteristics.

The result is shown in Fig. 19.45, and the mode boundaries are explicitly diagrammed in Fig. 19.46. It can be seen that, for operation above resonance, the only possible operating mode is the $k = 0$ CCM, and that the output voltage decreases monotonically with increasing switching frequency. Reduction in load current (or increase in load resistance, which decreases Q) causes the output voltage to increase. A number of successful designs that operate above resonance and utilize zero-voltage switching have been documented in the literature [7,21].

Operation below resonance is complicated by the presence of subharmonic and discontinuous conduction modes. The $k = 1$ CCM and $k = 2$ DCM are well behaved, in that the output voltage increases monotonically with increasing switching frequency. Increase of the load current again causes the output voltage to decrease. Successful designs that operate in these modes and employ zero-current switching are numerous. However, operation in the higher-order modes ($k = 2$ CCM, $k = 4$ DCM, etc.) is normally avoided.

Given F and Q, the operating mode can be evaluated directly, using the following algorithm. First, the continuous conduction mode k corresponding to operation at frequency F with heavy loading is found:

$$k = \text{INT}\left(\frac{1}{F}\right) \tag{19.90}$$

where INT(x) denotes the integer part of x. Next, the quantity k_1 is determined:

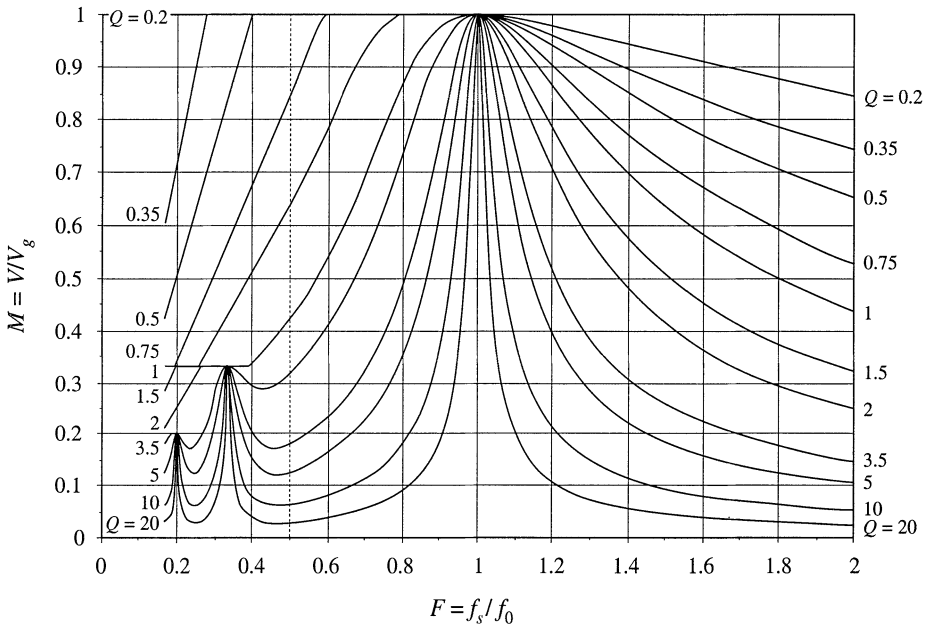

Fig. 19.45 Complete control plane characteristics of the series resonant converter, for the range $0.2 \le F \le 2$.

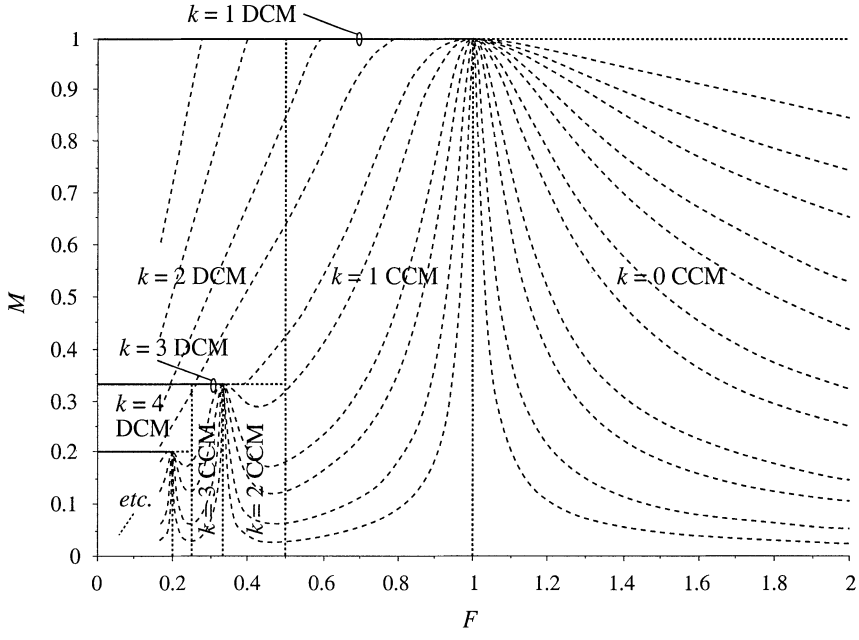

Fig. 19.46 Continuous and discontinuous conduction mode boundaries.

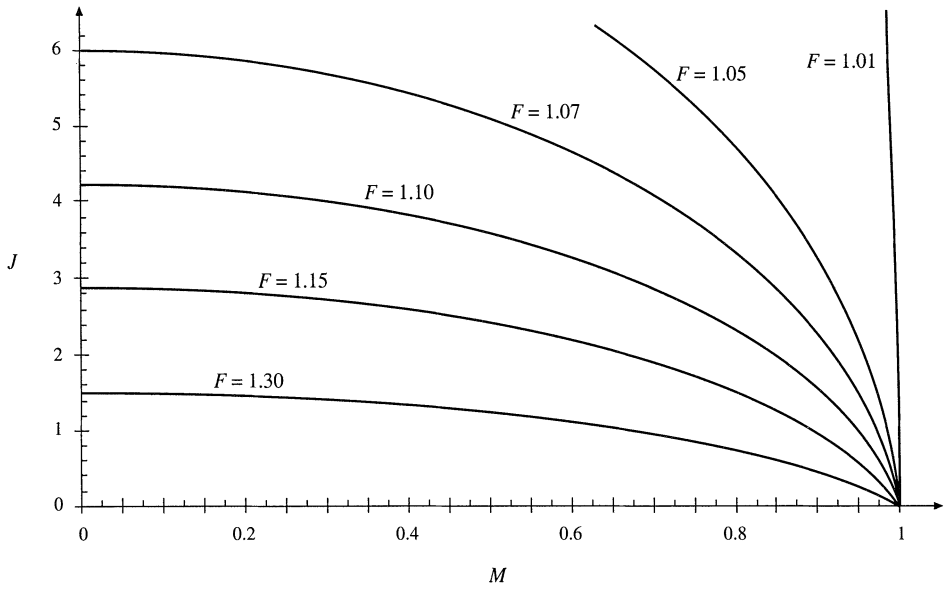

Fig. 19.47 Output characteristics, $k = 0$ CCM (above resonance).

$$k_1 = \text{INT}\left(\frac{1}{2} + \sqrt{\frac{1}{4} + \frac{Q\pi}{2F}}\right) \tag{19.91}$$

The converter operates in type k CCM provided that:

$$k_1 > k \tag{19.92}$$

Otherwise, the converter operates in type k_1 DCM. A simple algorithm can therefore be defined, in which the conversion ratio M is computed for a given F and Q. First, Eqs. (19.90) to (19.92) are evaluated, to determine the operating mode. Then, the appropriate equation (19.83), (19.85), or (19.88) is evaluated to find M.

Output I–V plane characteristics for the $k = 0$ CCM, plotted using Eq. (19.79), are shown in Fig. 19.47. The constant-frequency curves are elliptical, and all pass through the point $M = 1$, $J = 0$. For a given switching frequency, the operating point is given by the intersection of the elliptical converter output characteristic with the load I–V characteristic.

Output plane characteristics that combine the $k = 1$ CCM, $k = 1$ DCM, and $k = 2$ DCM are shown in Fig. 19.48. These were plotted using Eqs. (19.79), (19.85), and (19.88). These curves were plotted with the assumption that the transistors are allowed to conduct no longer than one tank half-cycle during each switching half-period; this eliminates subharmonic modes and causes the converter to operate in $k = 2$ or $k = 1$ DCM whenever $f_s < 0.5f_0$. It can be seen that the constant-frequency curves are elliptical in the continuous conduction mode, vertical (voltage source characteristic) in the $k = 1$ DCM, and horizontal (current source characteristic) in the $k = 2$ DCM.

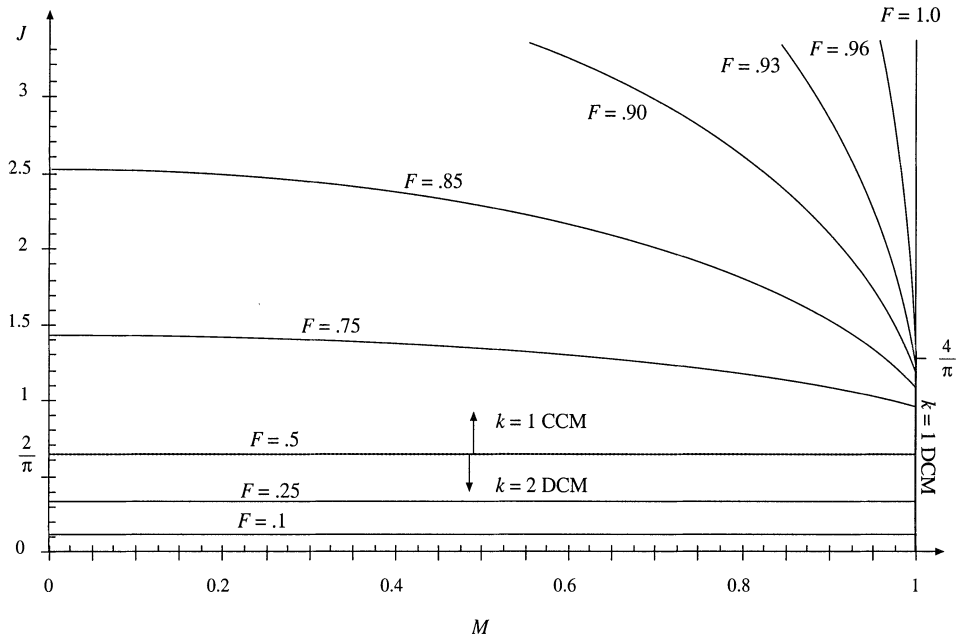

Fig. 19.48 Output characteristics, $k = 1$ CCM, $k = 1$ DCM, and $k = 2$ DCM (below resonance).

19.5.2 Parallel Resonant Converter

For operation in the frequency range $0.5f_0 < f_s < \infty$, the parallel resonant dc–dc converter exhibits one continuous conduction mode and one discontinuous conduction mode. Typical CCM switch voltage $v_s(t)$, tank inductor current $i_L(t)$, and tank capacitor voltage $v_C(t)$ waveforms are illustrated in Fig. 19.49. The CCM converter output characteristics are given by

$$M = \left(\frac{2}{\gamma}\right)\left(\varphi - \frac{\sin(\varphi)}{\cos\left(\frac{\gamma}{2}\right)}\right) \tag{19.93}$$

$$\varphi = \begin{cases} -\cos^{-1}\left(\cos\left(\frac{\gamma}{2}\right) + J\sin\left(\frac{\gamma}{2}\right)\right) & \text{for } 0 < \gamma < \pi \text{ (above resonance)} \\ +\cos^{-1}\left(\cos\left(\frac{\gamma}{2}\right) + J\sin\left(\frac{\gamma}{2}\right)\right) & \text{for } \pi < \gamma < 2\pi \text{ (below resonance)} \end{cases} \tag{19.94}$$

and where M, J, and γ are again defined as in Eqs. (19.80) and (19.81). Given the normalized load current J and the half-switching-period-angle γ, one can evaluate Eq. (19.94) to find φ, and then evaluate Eq. (19.93) to find the converter voltage conversion ratio M. In other words, the output voltage can be found for a given load current and switching frequency, without need for computer iteration.

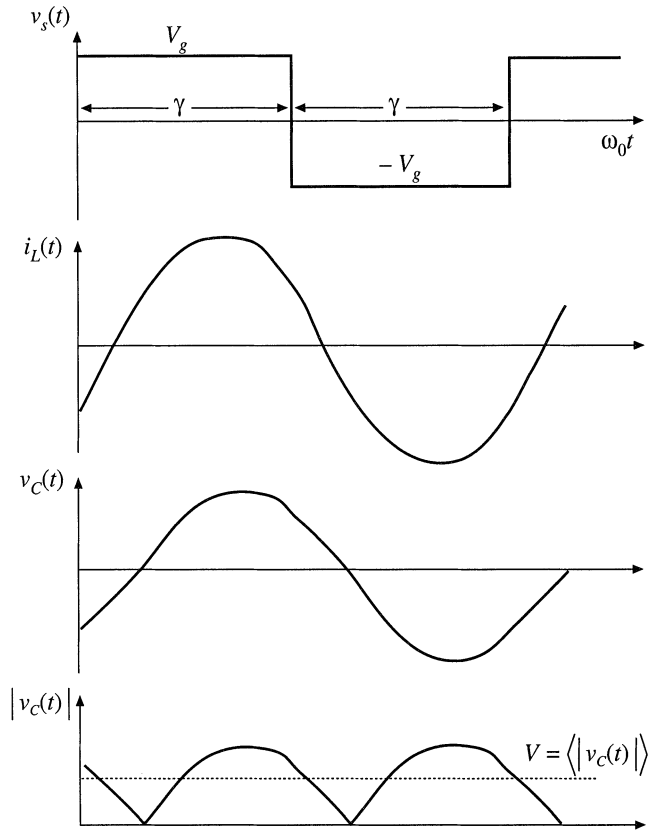

Fig. 19.49 Typical waveforms of the parallel resonant converter, operating in the continuous conduction mode.

A discontinuous conduction mode mechanism occurs in the parallel resonant converter which is the dual of the discontinuous conduction mode mechanism of the series resonant converter. In this mode, a discontinuous subinterval occurs in which all four output bridge rectifier diodes are forward-biased, and the tank capacitor voltage remains at zero. This mode occurs both above and below resonance when the converter is heavily loaded. Typical DCM tank capacitor voltage and inductor current waveforms are illustrated in Fig. 19.50. The condition for operation in the discontinuous conduction mode is

$$\begin{aligned} J &> J_{crit}(\gamma) \quad \text{for DCM} \\ J &< J_{crit}(\gamma) \quad \text{for CCM} \end{aligned} \tag{19.95}$$

where

$$J_{crit}(\gamma) = -\frac{1}{2}\sin(\gamma) + \sqrt{\sin^2\left(\frac{\gamma}{2}\right) + \frac{1}{4}\sin^2(\gamma)} \tag{19.96}$$

The discontinuous conduction mode is described by the following set of equations:

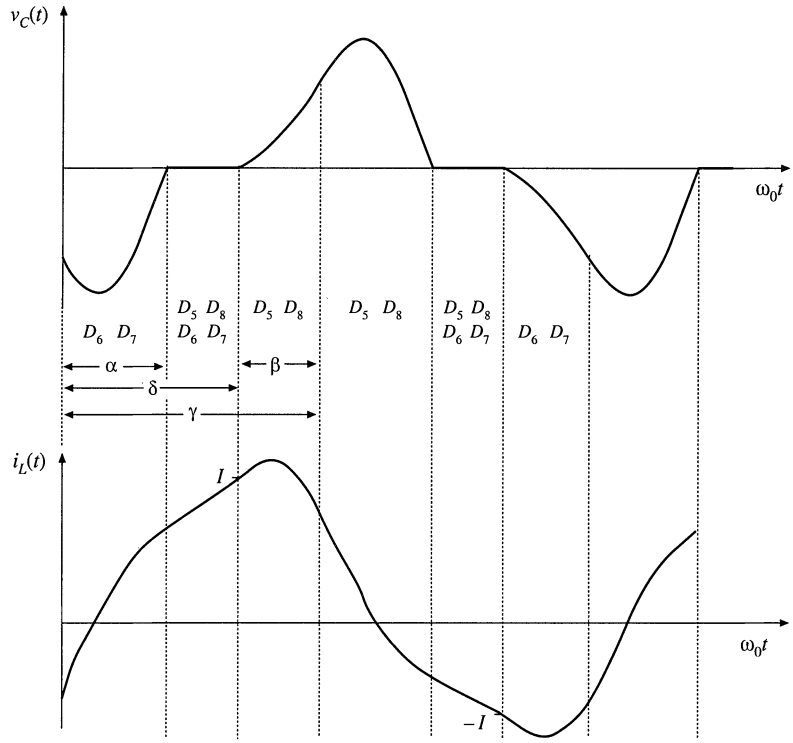

Fig. 19.50 Typical waveforms of the parallel resonant converter, operating in the discontinuous conduction mode.

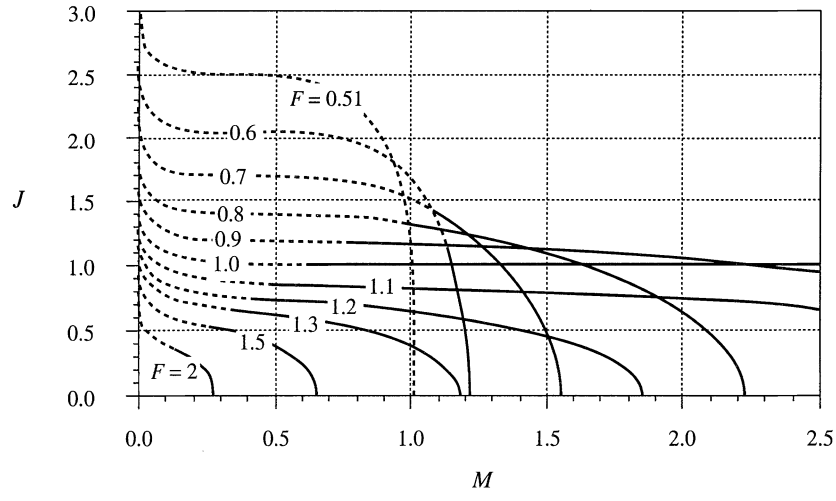

Fig. 19.51 Exact output characteristics of the parallel resonant converter, for $F > 0.5$. Solid curves: CCM, dashed curves: DCM.

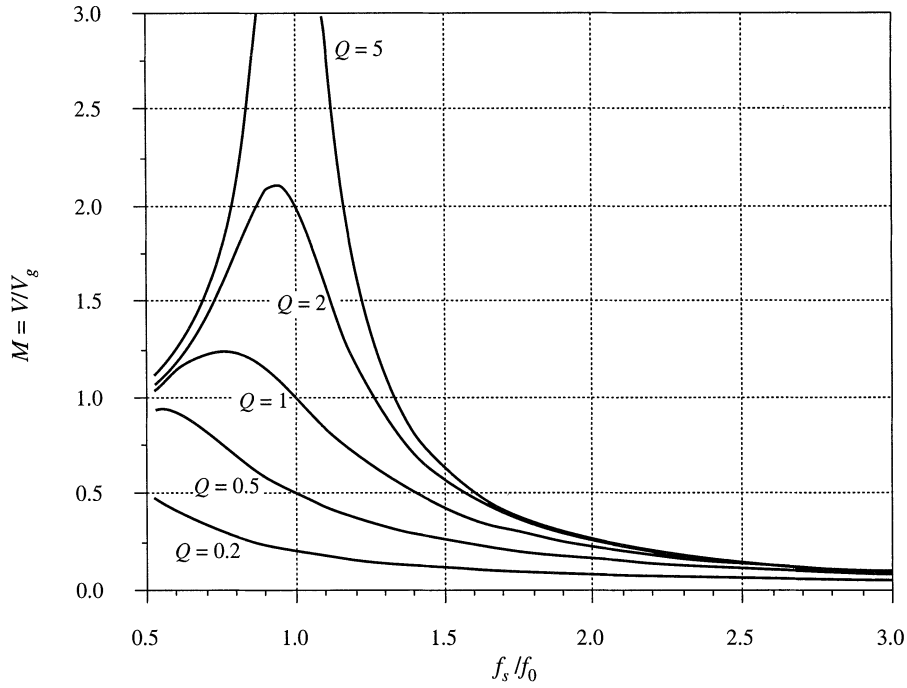

Fig. 19.52 Exact control characteristics of the parallel resonant converter, with a resistive load. Both CCM and DCM operation is included, for $0.5 \le F \le 3$.

$$\begin{aligned} M_{C0} &= 1 - \cos(\beta) \\ J_{L0} &= J + \sin(\beta) \\ \cos(\alpha + \beta) - 2\cos(\alpha) &= -1 \\ -\sin(\alpha + \beta) + 2\sin(\alpha) + (\delta - \alpha) &= 2J \\ \beta + \delta &= \gamma \\ M &= 1 + \left(\frac{2}{\gamma}\right)(J - \delta) \end{aligned} \tag{19.97}$$

Unfortunately, the solution to this set of equations is not known in closed form, because of the mixture of linear and trigonometric terms. In consequence, the equations must be solved iteratively. For a given γ and J, a computer is used to iteratively find the angles α, β, and δ. M is then evaluated, and the output plane characteristics can be plotted. The result is given in Fig. 19.51. The dashed lines are the DCM solutions, and the solid lines are the valid CCM solutions. Figure 19.51 describes the complete dc behavior of the ideal parallel resonant converter for all switching frequencies above $0.5f_0$. For given values of normalized switching frequency $F = f_s/f_0 = \pi/\gamma$, the relationship between the normalized output current J and the normalized output voltage M is approximately elliptical. At resonance ($F = 1$), the CCM ellipse degenerates to the horizontal line $J = 1$, and the converter exhibits current source characteristics. Above resonance, the converter can both step up the voltage ($M > 1$) and step down the voltage ($M < 1$). The normalized load current is then restricted to $J < 1$, corresponding to $I < V_g/nR_0$. For a given switching frequency greater than the resonant frequency, the actual limit on maximum load current is even more restrictive than this limit. Below resonance, the converter can also step up and step down the volt-

age. Normalized load currents J greater than one are also obtainable, depending on M and F. However, no solutions occur when M and J are simultaneously large.

In Fig. 19.52, the control plane characteristics are plotted for a resistive load. The parameter Q is defined for the parallel resonant converter as $Q = R/n^2R_0$. The normalized load current is then given by $J = M/Q$.

19.6 SUMMARY OF KEY POINTS

1. The sinusoidal approximation allows a great deal of insight to be gained into the operation of resonant inverters and dc–dc converters. The voltage conversion ratio of dc–dc resonant converters can be directly related to the tank network transfer function. Other important converter properties, such as the output characteristics, dependence (or lack thereof) of transistor current on load current, and zero-voltage- and zero-current-switching transitions, can also be understood using this approximation. The approximation is accurate provided that the effective Q factor is sufficiently large, and provided that the switching frequency is sufficiently close to resonance.
2. Simple equivalent circuits are derived, which represent the fundamental components of the tank network waveforms, and the dc components of the dc terminal waveforms.
3. Exact solutions of the ideal dc–dc series and parallel resonant converters are listed here as well. These solutions correctly predict the conversion ratios, for operation not only in the fundamental continuous conduction mode, but in discontinuous and subharmonic modes as well.
4. Zero-voltage switching mitigates the switching loss caused by diode recovered charge and semiconductor device output capacitances. When the objective is to minimize switching loss and EMI, it is preferable to operate each MOSFET and diode with zero-voltage switching.
5. Zero-current switching leads to natural commutation of SCRs, and can also mitigate the switching loss due to current tailing in IGBTs.
6. The input impedance magnitude $\| Z_i \|$, and hence also the transistor current magnitude, are monotonic functions of the load resistance R. The dependence of the transistor conduction loss on the load current can be easily understood by simply plotting $\| Z_i \|$ in the limiting cases as $R \rightarrow \infty$ and as $R \rightarrow 0$, or $\| Z_{i\infty} \|$ and $\| Z_{i0} \|$.
7. The ZVS/ZCS boundary is also a simple function of $Z_{i\infty}$ and Z_{i0}. If ZVS occurs at open-circuit and at short-circuit, then ZVS occurs for all loads. If ZVS occurs at short-circuit, and ZCS occurs at open-circuit, then ZVS is obtained at matched load provided that $\| Z_{i\infty} \| > \| Z_{i0} \|$.
8. The output characteristics of all resonant inverters considered here are elliptical, and are described completely by the open-circuit transfer function magnitude $\| H_\infty \|$, and the output impedance $\| Z_{o0} \|$. These quantities can be chosen to match the output characteristics to the application requirements.

REFERENCES

[1] F.C. SCHWARZ, "An Improved Method of Resonant Current Pulse Modulation for Power Converters," *IEEE Power Electronics Specialists Conference*, 1975 Record, pp. 194–204, June 1975.

[2] R.L. STEIGERWALD, "High Frequency Resonant Transistor Dc-Dc Converters," *IEEE Transactions on Industrial Electronics*, Vol. 31, No. 2, pp. 181–191, May 1984.

[3] M. COSBY and R. NELMS, "Designing a Parallel-Loaded Resonant Inverter for an Electronic Ballast Using

the Fundamental Approximation," *IEEE Applied Power Electronics Conference*, 1993 Record, pp. 413–423.

[4] M. GULKO and S. BEN-YAAKOV, "Current-Sourcing Push-Pull Parallel-Resonance Inverter (CS-PPRI): Theory and Application as a Fluorescent Lamp Driver," *IEEE Applied Power Electronics Conference*, 1993 Record, pp. 411–417.

[5] Y. CHERON, H. FOCH, and J. SALESSES, "Study of a Resonant Converter Using Power Transistors in a 25kW X-ray Tube Power Supply," *IEEE Power Electronics Specialists Conference*, Proceedings ESA Sessions, pp. 295–306, June 1985.

[6] S. D. JOHNSON, A. F. WITULSKI, and R. W. ERICKSON, "A Comparison of Resonant Topologies in High Voltage Applications," *IEEE Transactions on Aerospace and Electronic Systems*, Vol. 24, No. 3, pp. 263–274, July 1988.

[7] Y. MURAI and T. A. LIPO, "High Frequency Series Resonant Dc Link Power Conversion," *IEEE Industry Applications Society Annual Meeting*, 1988 Record, pp. 648–656.

[8] F. C. SCHWARZ, "A Doublesided Cyclo-Converter," *IEEE Power Electronics Specialists Conference*, 1979 Record, pp. 437–447.

[9] D. DIVAN, "The Resonant Dc Link Converter: A New Concept in Static Power Conversion," *IEEE Industry Applications Society Annual Meeting*, 1986 Record, pp. 648–656.

[10] R.L. STEIGERWALD, "A Comparison of Half-Bridge Resonant Converter Topologies," *IEEE Applied Power Electronics Conference*, 1987 Record, pp. 135–144.

[11] R. SEVERNS, "Topologies for Three Element Resonant Converters," *IEEE Applied Power Electronics Conference*, 1990 Record, pp. 712–722.

[12] M. KAZIMIERCZUK, W. SZARANIEC, and S. WANG, "Analysis and Design of Parallel Resonant Converter at High Q_L," *IEEE Transactions on Aerospace and Electronic Systems*, Vol. 28, pp. 35–50. January 1992.

[13] R. KING and T. STUART, "A Normalized Model for the Half Bridge Series Resonant Converter," *IEEE Transactions on Aerospace and Electronic Systems*, March 1981, pp. 180–193.

[14] V. VORPERIAN and S. ĆUK, "A Complete DC Analysis of the Series Resonant Converter," *IEEE Power Electronics Specialists Conference*, 1982 Record, pp. 85–100, June 1982.

[15] R. KING and T.A. STUART, "Inherent Overload Protection for the Series Resonant Converter," *IEEE Transactions on Aerospace and Electronic Systems*, Vol. 19, No. 6, pp. 820–830, Nov. 1983.

[16] A. WITULSKI and R. ERICKSON, "Steady-State Analysis of the Series Resonant Converter," *IEEE Transactions on Aerospace and Electronic Systems*, Vol. 21, No. 6, pp. 791–799, Nov. 1985.

[17] A. WITULSKI and R. ERICKSON, "Design of the Series Resonant Converter for Minimum Component Stress," *IEEE Transactions on Aerospace and Electronic Systems*, Vol. 22, No. 4, July 1986, pp. 356–363.

[18] R. ORUGANTI and F.C. LEE, "Resonant Power Processors, Part 1: State Plane Analysis," *IEEE Transactions on Industry Applications*, Vol. 21, Nov./Dec. 1985, pp. 1453–1460.

[19] C.Q. LEE and K. SIRI, "Analysis and Design of Series Resonant Converter by State Plane Diagram," *IEEE*

Transactions on Aerospace and Electronic Systems, Vol. 22, No. 6, pp. 757–763, November 1986.

[20] S. TRABERT and R. ERICKSON, "Steady-State Analysis of the Duty Cycle Controlled Series Resonant Converter," *IEEE Power Electronics Specialists Conference*, 1987 Record, pp. 545–556.

[21] K.D.T. NGO, "Analysis of a Series Resonant Converter Pulsewidth-Modulated of Current-Controlled for Low Switching Loss," *IEEE Power Electronics Specialists Conference*, 1987 Record, pp. 527–536, June 1987.

[22] R. ORUGANTI and F.C. LEE, "State Plane Analysis of the Parallel Resonant Converter," *IEEE Power Electronics Specialists Conference*, 1985 Record, pp. 56–73, June 1985.

[23] S. JOHNSON, "Steady-State Analysis and Design of the Parallel Resonant Converter," M.S. Thesis, University of Colorado, Boulder, 1986.

[24] S. JOHNSON and R. ERICKSON, "Steady-State Analysis and Design of the Parallel Resonant Converter," *IEEE Transactions on Power Electronics*, Vol. 3, No. 4, pp. 93–104, Jan. 1988.

[25] A. BHAT and M. SWAMY, "Analysis and Design of a High-Frequency Parallel Resonant Converter Operating Above Resonance," *IEEE Transactions on Aerospace and Electronic Systems*, Vol. 25, No. 4, July 1989, pp. 449–458.

[26] F.S. TSAI, P. MATERU, and F.C. LEE, "Constant Frequency, Clamped Mode Resonant Converters," *IEEE Power Electronics Specialists Conference*, 1987 Record, pp. 557–566, June 1987.

[27] V. VORPERIAN and S. ĆUK, "Small-Signal Analysis of Resonant Converters," *IEEE Power Electronics Specialists Conference*, 1983 Record, pp. 269–282, June 1983.

[28] V. VORPERIAN, "High-Q Approximation in the Small-Signal Analysis of Resonant Converters," *IEEE Power Electronics Specialists Conference*, 1985 Record, pp. 707–715.

[29] R. KING and T. STUART, "Small-Signal Model for the Series Resonant Converter," *IEEE Transactions on Aerospace and Electronic Systems*, May 1985, Vol. 21, No. 3, pp. 301–319.

[30] A. WITULSKI, A. HERNANDEZ, and R. ERICKSON, "Small-Signal Equivalent Circuit Modeling of Resonant Converters," *IEEE Transactions on Power Electronics*, January 1991.

[31] R. FISHER, K. NGO, and M. KUO, "A 500 kHz, 250 W Dc–dc Converter with Multiple Outputs Controlled by Phase-Shifted PWM and Magnetic Amplifiers," *Proceedings of High Frequency Power Conversion Conference*, pp. 100–110, May 1988.

[32] L. MWEENE, C. WRIGHT, and M. SCHLECHT, "A 1 kW, 500 kHz Front-End Converter for a Distributed Power Supply System," *IEEE Applied Power Electronics Conference*, 1989 Record, pp. 423–432.

[33] R. REDL, L. BELOGH, and D. EDWARDS, "Optimum ZVS Full-Bridge DC/DC Converter with PWM Phase-Shift Control: Analysis, Design Considerations, and Experimental Results," *IEEE Applied Power Electronics Conference*, 1994 Record, pp. 159–165.

[34] J. G. CHO, J. A. SABATE, and F. C. LEE, "Novel Full Bridge Zero-Voltage-Transition PWM DC/DC Converter for High Power Applications," *IEEE Applied Power Electronics Conference*, 1994 Record, pp. 143–149.

[35] O. D. PATTERSON and D. M. DIVAN, "Pseudo-Resonant Full Bridge DC/DC Converter," *IEEE Power Electronics Specialists Conference*, 1987 Record, pp. 424–430.

[36] R. FARRINGTON, M. JOVANOVIC, and F. C. LEE, "Analysis of Reactive Power in Resonant Converters," *IEEE Power Electronics Specialists Conference*, 1992 Record, pp. 197–205.

[37] R. D. MIDDLEBROOK, "Null Double Injection and the Extra Element Theorem," *IEEE Transactions on Education*, Vol. 32, No. 3, pp. 167–180, August 1989.

[38] D. TUTTLE, *Network Synthesis*, New York: John Wiley & Sons, Vol. 1, Chapter 6, 1958.

PROBLEMS

19.1 *Analysis of a half-bridge dc–dc parallel resonant converter, operated above resonance.* In Fig. 19.53, the elements C_b, L_F, and C_F are large in value, and have negligible switching ripple. You may assume that all elements are ideal. You may use the sinusoidal approximation as appropriate.

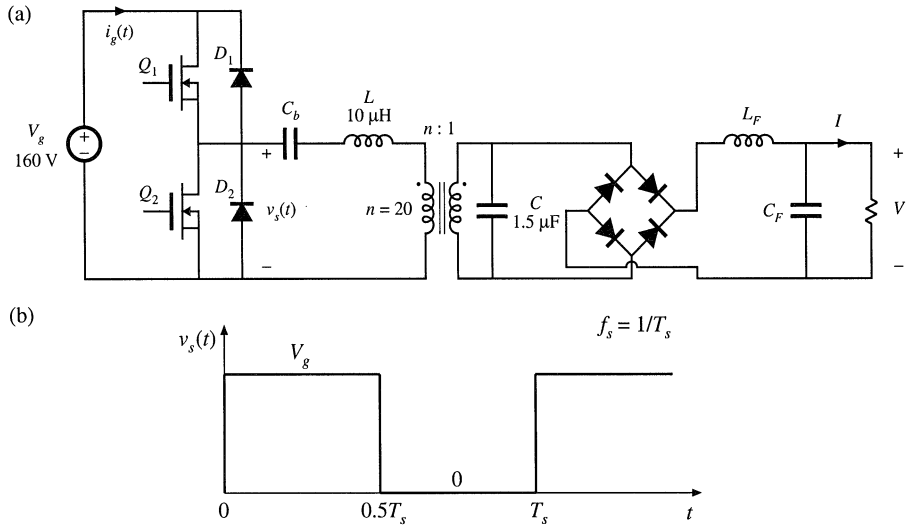

Fig. 19.53 Half-bridge parallel resonant converter of Problem 19.1: (a) schematic, (b) switch voltage waveform.

(a) Sketch the waveform of the current $i_g(t)$.

(b) Construct an equivalent circuit for this converter, similar to Fig. 19.22, which models the fundamental components of the tank waveforms and the dc components of the converter input current and output voltage. Clearly label the values and/or give expressions for all elements in your model, as appropriate.

(c) Solve your model to derive an expression for the conversion ratio $V/V_g = M(F, Q_e, n)$.

At rated (maximum) load, this converter produces $I = 20$ A at $V = 3.3$ V.

(d) What is the converter switching frequency f_s at rated load?

(e) What is the magnitude of the peak transistor current at rated load?

At minimum load, the converter produces $I = 2$ A at $V = 3.3$ V.

(f) What is the converter switching frequency f_s at minimum load?

(g) What is the magnitude of the peak transistor current at minimum load? Compare with your answer from part (e)—what happens to the conduction loss and efficiency at minimum load?

19.2 A dc–dc resonant converter contains an LCC tank network [Fig. 19.1(d)], with an output filter containing a filter inductor as in the parallel resonant dc–dc converter.

(a) Sketch an equivalent circuit model for this converter, based on the approximate sinusoidal analysis method of Section 19.1. Give expressions for all elements in your model.

(b) Solve your model, to derive an expression for the conversion ratio $M = V/V_g$. Express M as a function of $F = f_s/f_\infty$, $Q_e = R_e/R_0$, and $n = C_s/C_p$, where f_∞ is defined as in Eq. (19.50) and R_0 is

$$R_0 = \sqrt{\frac{L\left(C_s + C_p\right)}{C_s C_p}}$$

(c) Plot M vs. F, for $n = 1$ and $Q_e = 1$, 2, and 5.

(d) Plot M vs. F, for $n = 0.25$ and $Q_e = 1$, 2, and 5.

19.3 Dual of the series resonant converter. In the converter illustrated in Fig. 19.54, L_{F1}, L_{F2}, and C_F are large filter elements, whose switching ripples are small. L and C are tank elements, whose waveforms $i_L(t)$ and $v_C(t)$ are nearly sinusoidal.

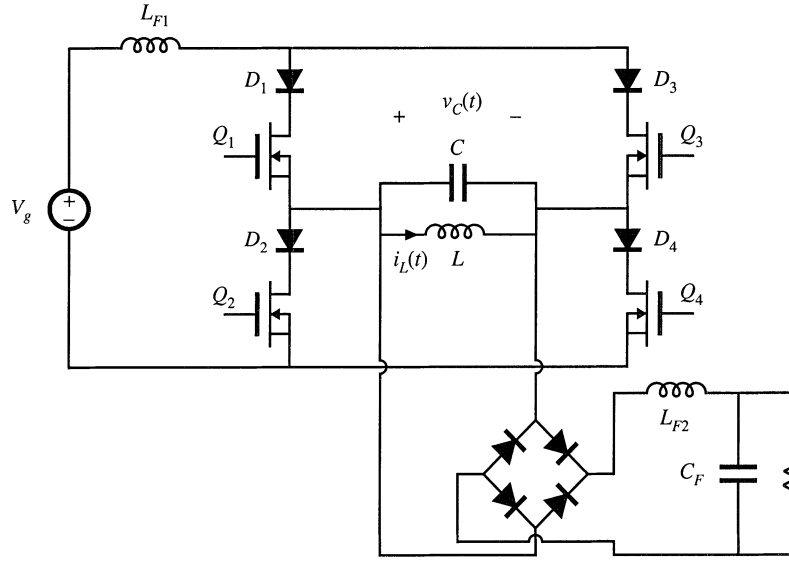

Fig. 19.54 Dual of the series resonant converter, Problem 19.3.

(a) Using the sinusoidal approximation method, develop equivalent circuit models for the switch network, tank network, and rectifier network.

(b) Sketch a Bode diagram of the parallel LC parallel tank impedance.

(c) Solve your model. Find an analytical solution for the converter voltage conversion ratio $M = V/V_g$, as a function of the effective Q_e and the normalized switching frequency $F = f_s/f_0$. Sketch M vs. F.

(d) What can you say about the validity of the sinusoidal approximation for this converter? Which

parts of your M vs. F plot of part (c) are valid and accurate?

19.4 The converter of Problem 19.3 operates below resonance.

(a) Sketch the waveform $v_C(t)$. For each subinterval, label: (*i*) which of the diodes D_1 to D_4 and transistors Q_1 to Q_4 conduct current, and (*ii*) which devices block voltage.

(b) Does the reverse recovery process of diodes D_1 to D_4 lead to switching loss? Do the output capacitances of transistors Q_1 to Q_4 lead to switching loss?

(c) Repeat parts (a) and (b) for operation above resonance.

19.5 A parallel resonant converter operates with a dc input voltage of $V_g = 270$ V. The converter supplies 5 V to a dc load. The dc load power varies over the range 20 W to 200 W. It is desired to operate the power transistors with zero voltage switching. The tank element values are $L = 57$ μH, $C_p = 0.9$ nF, referred to the transformer primary. The parallel resonant tank network contains an isolation transformer having a turns ratio of 52:1.

(a) Define F as in Eq. (19.19). Derive an expression for F, as a function of M and Q_e.

(b) Determine the switching frequency, peak transistor current, and peak tank capacitor voltage at the maximum load power operating point.

(c) Determine the switching frequency, peak transistor current, and peak tank capacitor voltage at the minimum load power operating point.

19.6 In a certain resonant inverter application, the dc input voltage is $V_g = 320$ V. The inverter must produce an approximately sinusoidal output voltage having a frequency of 200 kHz. Under no load (output open-circuit) conditions, the inverter should produce a peak-to-peak output voltage of 1500 V. The nominal resistive operating point is 200 Vrms applied to 100 Ω. A nonisolated LCC inverter is employed. It is desired that the inverter operate with zero-voltage switching, at least for load resistances less than 200 Ω.

(a) Derive expressions for the output open-circuit voltage V_{oc} and short-circuit current I_{sc} of the LCC inverter. Express your results as functions of $F = f_s/f_\infty$, V_g, $R_\infty = L/C_s \| C_p$ and $n = C_s/C_p$. The open-circuit resonant frequency f_∞ is defined in Eq. (19.50).

(b) To meet the given specifications, how should the short-circuit current I_{sc} be chosen?

(c) Specify tank element values that meet the specifications.

(d) Under what conditions does your design operate with zero-voltage switching?

(e) Compute the peak transistor current under no-load and short-circuit conditions.

19.7 A series resonant dc–dc converter operates with a dc input voltage of $V_g = 550$ V. The converter supplies 30 kV to a load. The dc load power varies over the range 5 kW to 25 kW. It is desired to operate the power transistors with zero-voltage switching. The maximum feasible switching frequency is 50 kHz. An isolation transformer having a $1:n$ turns ratio is connected in series with the tank network. The peak tank capacitor voltage should be no greater than 2000 V, referred to the primary.

(a) Derive expressions for the peak tank capacitor voltage and peak tank inductor current.

(b) Select values for the tank inductance, tank capacitance, and turns ratio, such that the given specifications are met. Attempt to minimize the peak tank inductor current, while maximizing the worst-case minimum switching frequency.

19.8 Figure 19.55 illustrates a full-bridge resonant inverter containing an LLC tank network.

(a) Sketch the Bode diagrams of the input impedance under short-circuit and open-circuit conditions: $\| Z_{i0}(j\omega) \|$ and $\| Z_{i\infty}(j\omega) \|$. Give analytical expressions for the resonant frequencies and asymptotes.

(b) Describe the conditions on switching frequency and load resistance that lead to zero-voltage switching.

(c) Derive an expression for the frequency f_m, where $\| Z_{i0} \| = \| Z_{i\infty} \|$.

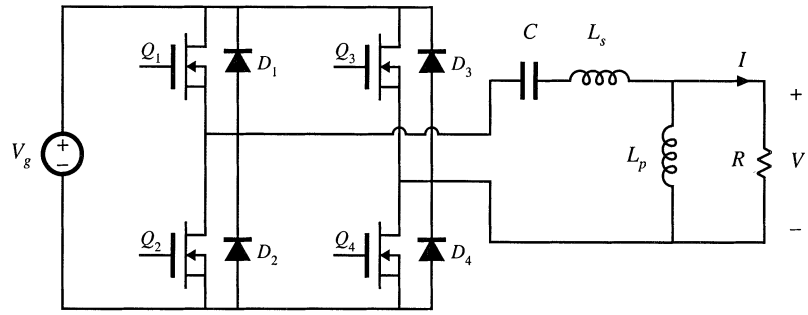

Fig. 19.55 LLC inverter of Problem 19.8.

(d) Sketch the Bode plot of $\| H_\infty(j\omega) \|$. Label the resonant frequency, and give analytical expressions for the asymptotes.

19.9 You are given the LLC inverter circuit of Fig. 19.56. Under nominal conditions, this converter operates at switching frequency $f_s = 100$ kHz. All elements are ideal.

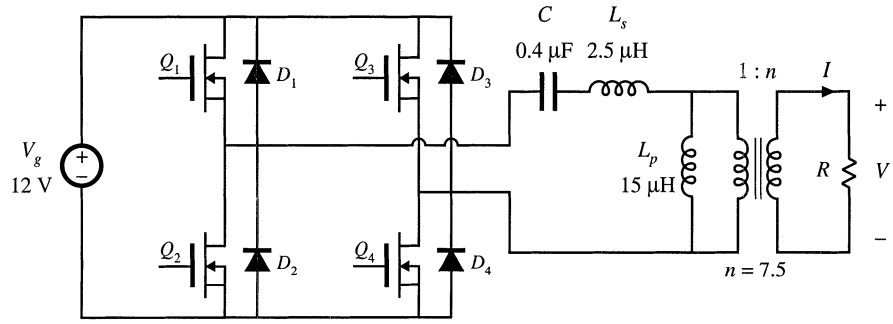

Fig. 19.56 Transformer-isolated LLC inverter, Problem 19.9.

(a) Determine the numerical values of the open-circuit peak output voltage V_{oc} and the short-circuit peak output current I_{sc}.

(b) Sketch the elliptical output characteristic. Over what portion of this ellipse does the converter operate with zero-voltage switching? Does it operate with zero-voltage switching at matched load?

(c) Sketch the Bode plots of $\| Z_{i\infty} \|$ and $\| Z_{i0} \|$, and label the numerical values of f_0, f_∞, f_m, and f_s.

(d) What is the numerical value of the peak transistor current when $R = 0$? When $R \to \infty$?

(e) The inverter operates with load resistances that can vary between 500 Ω and an open circuit. What is the resulting range of output voltage? Does the inverter always operate with zero-voltage switching?

19.10 It is desired to obtain a converter with current source characteristics. Hence, a series resonant converter is designed for operation in the $k = 2$ discontinuous conduction mode. The switching frequency is chosen to be $f_s = 0.225 f_0$, where f_0 is the tank resonant frequency (consider only open-loop operation). The load R is a linear resistance which can assume any positive value: $0 \le R < \infty$.

(a) Plot the output characteristics (M vs. J), for all values of R in the range $0 \le R < \infty$. Label mode boundaries, evaluate the short-circuit current, and give analytical expressions for the output characteristics.

(b) Over what range of R (referred to the tank characteristic impedance R_0) does the converter operate as intended, in the $k = 2$ discontinuous conduction mode?

19.11 The parallel resonant converter as a single-phase high-quality rectifier. It is desired to utilize a transformer-isolated parallel resonant dc–dc converter in a single-phase low-harmonic rectifier system. By properly varying the converter switching frequency, a near-ideal rectifier system that can be modeled as in Fig. 18.12 is obtained. You may utilize the results of Section 19.5.2 to answer this problem. The parallel resonant tank network contains an isolation transformer having a $1:n$ turns ratio. You may use either approximate graphical analysis or computer iteration to answer parts (b) and (c).

(a) Plot the normalized input characteristics (normalized input voltage $m_g = nv_g/v$ vs. normalized input current $j_g = i_g nR_0/v$) of the parallel resonant converter, operated in the continuous conduction mode above resonance. Plot curves for $F = f_s/f_0 = 1.0$, 1.1, 1.2, 1.3, 1.5, and 2.0. Compare these characteristics with the desired linear resistive input characteristic $v_g/i_g = R_{emulated}$.

(b) The converter is operated open-loop, with $F = 1.1$. The applied normalized input voltage is a rectified sinusoid of unity magnitude: $m_g(t) = |\sin(\omega t)|$. Sketch the resulting normalized input current waveform $j_g(t)$. Approximately how large is the peak current? The crossover dead time?

(c) A feedback loop is now added, which regulates the input current to follow the input voltage such that $i_g(t) = v_g(t)/R_{emulated}$. You may assume that the feedback loop operates perfectly. For the case $R_{emulated} = R_0$, and with the same applied $m_g(t)$ waveform as in part (b), sketch the switching frequency waveform for one ac line period [i.e., show how the controller must vary F to regulate $i_g(t)$]. What is the maximum value of F? *Note*: In practice, the converter would be designed to operate with a smaller peak value of j_g, so that the switching frequency variations would be better behaved.

(d) Choose element values (tank inductance, tank capacitance, and transformer turns ratio) such that the converter of part (c) meets the following specifications:

Ac input voltage	120 Vrms, 60 Hz
Dc output voltage	42 V
Average power	800 W
Maximum switching frequency	200 kHz

Refer the element values to the primary side of the transformer.